Design of an Improved Moisture Separator in a Turbocharger System for Fuel Cells

A Thesis
Presented to
The Academic Faculty

by

Jacob R. Aspinwall

In Partial Fulfillment
of the Requirements for the Degree
Master of Science in Mechanical Engineering

Georgia Institute of Technology
July 2004

Design of an Improved Moisture Separator for PEM Fuel Cell Applications

Approved By:

Sheldon Jeter, Co-Advisor

Said I. Abdel-Khalik, Co-Advisor

Srinivas Garimella

S. Mostafa Ghiaasiaan

Date Approved: 26 April 2004

Table of Contents

List of Tables

List of Figures

Summary

Moisture recovery is important in the operation of many fuel cell systems, especially proton exchange membrane (PEM) fuel cells. The exhaust of a PEM fuel cell is a moderate temperature, pressurized humid air stream. A system that recovers liquid water condensate from the pressurized humid exhaust stream of a PEM fuel cell would markedly increase the effectiveness of such a system. The recovered water could be used to hydrate the fuel cell membrane, and it could supply a hydrocarbon reformer used for generating hydrogen.

The goal of this project is to investigate and document moisture recovery from the simulated humid exhaust stream of a 25 kW fuel cell with an improved axial flow separator. An axial flow centrifugal separator design was chosen as the best candidate due to its high efficiency and low pressure drop and a prototype was designed and constructed. The separator was then integrated into an experimental test system. First, the stream was simulated by heating compressed air and then humidifying it with superheated steam. Then, after expanding through the turbine section of an automotive turbocharger, the humid stream was passed through the moisture separator where liquid water condensate was removed from the flow. Results are presented for varying turbine inlet conditions at three separate separation lengths. It is shown that the separation efficiency for the improved design was 40% higher and the pressure drop was only 1/3 that of the conventional separator.

Chapter I

Introduction

The purpose of this investigation is to develop and document an improved moisture recovery device for use in automotive fuel cell applications. Water is a byproduct of the energetic reaction that occurs at the electrodes of Proton Exchange Membrane (PEM) fuel cells and is removed from the fuel cell in the pressurized exhaust stream. Upon removing the moisture, the stream then becomes a pressurized humid air stream. A system that recovers liquid water condensate in addition to energy from the pressurized humid exhaust of a PEM fuel cell would markedly increase the effectiveness of such a system. The recovered water could be used to maintain proper hydration of the PEM membrane, and it could supply a hydrocarbon reformer used for generating hydrogen.

Prior research has shown that a turbocharger used in tandem with a conventional centrifugal moisture separator can successfully extract work from the pressurized exhaust of a PEM fuel cell while removing moisture from the humid stream (McTaggert *et al.,* 1998). This research will attempt to utilize an axial flow centrifugal separator to increase the separation efficiency of the system. For this purpose, an axial flow separator prototype was designed and constructed, and its performance evaluated and compared to that of a conventional tangential separator.

A test apparatus that simulated the hot and humid exhaust stream of a PEM fuel

cell was used in this investigation. The apparatus utilizes an electric boiler to inject a carefully metered flow of steam into a pressurized stream of dry air. The air stream is supplied from a compressed air line at a set pressure and flow rate. The air is heated by in-line finned tube resistance heaters before being injected with steam. Once mixed, the humid air stream is directed through the turbine side of an automotive turbocharger. The turbine extracts energy from the expanding flow and converts it to shaft work used by the compressor side of the turbocharger. The expansion through the turbine also causes a drop in temperature and pressure of the humid stream which results in liquid water condensing in the stream. This condensate is subsequently removed from the stream by means of an axial flow centrifugal separator.

The experimental apparatus was instrumented to allow for measurements necessary in the evaluation of separator performance. These measurements include dry air mass flow rate, injected steam mass flow rate, turbine inlet/outlet conditions, and separator inlet/outlet conditions. In addition, several other temperature and pressure measurements were made to insure the proper operation of the experimental apparatus.

The remainder of this thesis is organized in the following manner. Chapter II contains background information on fuel cells as well as rationale for the selection of operating conditions chosen for this investigation. Chapter III presents summaries of the literature reviewed for this investigation. This includes literature on fuel cell and moisture recovery fundamentals. Chapter IV provides in-depth details and schematics of the experimental apparatus and improved moisture separator. Chapter V discusses the

experimental procedure used during the investigation. Chapter VI details the development of the improved separator and Chapter VII presents the experimental results and compares the improved separator with the conventional separator. Chapter VIII provides discussion and recommendations for further investigation.

Chapter II

Background

The background chapter provides information on fuel cells and establishes behind the choice of operating parameters for the experimental apparatus. The goal in this investigation is to develop an improved moisture separator for the recovery of liquid water condensate from the humid exhaust of a PEM fuel cell. This chapter presents information on PEM fuel cell operating requirements that is essential for the determination of exhaust conditions. The background information presented here includes information on fuel cell principles, hydrocarbon reformers, and fuel cell efficiency.

II.1 Fuel Cell Principles

Fuel cells produce electricity by means of an electrochemical reaction involving hydrogen and oxygen. Byproducts include water and heat. A fuel cell typically contains three components: an anode, cathode, and an electrolyte. The anode is the negative post of the fuel cell while the cathode is the positive post. The electrolyte conducts both positive ions to the cathode and negative ions to the anode. Fuel cell electrodes facilitate ionization and de-ionization of fuel and oxidants and provide a permeable interface between ions and electrolyte (EG&G, 2002). During operation, the fuel passes over the anode while an oxidant passes over the cathode.

Electric potential is generated when the fuel, usually gaseous hydrogen (H_2) splits into two positive ions (H^+) and two electrons (e^-). The electrons are drawn through an external circuit performing useful work and then return to the cathode. At the cathode the oxidant, usually gaseous oxygen (O_2), forms two oxygen atoms with strong negative charge. A negatively charged oxygen atom draws the two hydrogen atoms through a membrane and then combines with the two hydrogen ions forming water. The water byproducts are removed by excess oxidant. Equations 2.1 and 2.2 represent the reactions at the anode and cathode side of the fuel cell. Equation 2.3 represents the net reaction of the fuel cell (Hirshenhofer *et al.,* 1998).

$$2H_2 \Rightarrow 4H^+ + 4e^- \quad (2.1)$$

$$O_2 + 4H^+ + 4e^- \Rightarrow 2H_2O \quad (2.2)$$

$$2H_2 + O_2 \Rightarrow 2H_2O + \text{energy} \quad (2.3)$$

II.2 Fuel Cell Types

There are five main types of fuel cells and each type is generally classified by the type of electrolyte used. The various fuel cell types require different operating conditions and consequently have different applications. Of primary interest is the operating temperature for the fuel cell. Phosphoric Acid Fuel Cells (PAFC) use 100% concentrated phosphoric acid as the electrolyte and operate between 150 to 220 °C (302 to 428 °F). Molten Carbonate Fuel Cells (MCFC) use a molten salt as the electrolyte and operate between 600 and 700 °C (1112 to 1292 °F). Solid Oxide Fuel Cells (SOFC) use a non-

porous metal oxide as the electrolyte and operate at around 1000 °C (1832 °F). The high operating temperatures and longer warm up times of the PAFC, MCFC, and SOFC make the commercialization of these devices for automotive use unlikely. They are more likely to find applications in small-scale stationary electricity generation in the case of the PAFC or in large-scale stationary electricity generation in the case of the MCFC and SOFC. There is another type of fuel cell, the Alkaline Fuel Cell (AFC), which is also one of the oldest designs. Due to susceptibility to contamination, it requires pure hydrogen and oxygen which makes it expensive. Again, the AFC is unlikely to be developed for automotive use (EG&G, 2002).

The Proton Exchange Membrane Fuel Cell (PEMFC) is the most promising choice for automotive applications. The electrolyte is a fluorinated sulfonic acid polymer (Hirshenhofer *et al.,* 1998). This polymer requires adequate hydration however to function at peak performance. PEM fuel cells operate between 70 and 80 °C (158 and 176 °F) and 3.1 bar (30 psig). PEM fuel cells employ a platinum catalyst to promote the reaction between fuel and oxidant. Recent developments in material technology have decreased the cost of the platinum from prohibitive levels. Other improvements have increased the power density of these fuel cells to between 0.1 and 0.75 W/cm^2 making them particularly attractive for mobile electricity generation.

II.3 PEM Fuel Cell

This section will discuss the operating requirements and exhaust conditions of a

25 kW PEM fuel cell. Information on fuel supply and efficiency of an available 5 kW fuel cell system has been made available (Amphlett *et al.,* 1993). Results from this section will provide the design parameters that the experimental apparatus must meet to simulate the humid exhaust stream as well as give insight into the recovery requirements of the moisture separator in regard to fuel cell and external reformer hydration.

II.3.1 PEM Fuel Cell Operating Requirements

This investigation aims to utilize the water recovered from the hot humid exhaust from a PEM fuel cell with an external reformer to maintain proper hydration levels in the system at steady state. A chemical and mass balance performed on the system provides the amount of water that must be recovered. The fuel cell information that is provided details operation requirements for a typical 5 kW PEM fuel cell with a diesel fuel reformer. Operating conditions for a 25 kW PEM fuel cell are extrapolated from the 5 kW PEM fuel cell data. Both sets of values can be found in Table 2.1.

Table 2.1 Data on Fuel Cell Operating Conditions

	Given Data 5 kW Fuel Cell	Correlated Data 25 kW Fuel Cell
H_2 Feed Rate (mol/min)	3.1	15.5
H_2 Fuel Utilization	80%	80%
Excess Air	150%	150%
Fuel Cell Operating Pressure (psig)	30	30

The fuel supply rate to the reformer can be determined with the aid of the

stoichiometric equation shown in Equation 2.4 (Hirshenhofer *et al.,* 1998). Equation 2.4 shows that for every mole of diesel fuel supplied to the reformer, 24 moles of water are required resulting in 37 moles of hydrogen available to the fuel cell. In addition, the fuel cell generates one mole of water for every mole of hydrogen supplied as shown in Equation 2.3. The fuel flow rate for a 25 kW fuel cell as shown in Table 2.1 is 15.5 mol/min. The corresponding water supply rate to the reformer then is 10.1 mol/min. The efficiency of the PEM fuel cell in converting the hydrogen to actual use is only 80% so only 12.4 mol-H_2/min is actually used (Amphlett *et al.,* 1993). Since the H_2O generation to H_2 supply ratio is 1 to 1 from Equation 2.3, then the H_2O generation rate in the example 25 kW fuel cell is 12.4 mol/min. So, approximately 81% of the water available in the fuel cell exhaust stream must be recovered to supply the requirements of the reformer.

$$C_{12}H_{26} + 24H_2O \Rightarrow 12CO_2 + 37H_2 \tag{2.4}$$

It is also necessary to determine the amount of water available in the pressurized fuel cell stream. Equation 2.5 shows the reaction in the fuel cell cathode assuming 150% excess air. The molar usage rate of H_2 in the fuel cell is used in combination with Equation 2.5 to determine the mass flow rates of water and air for the conditions given in Table 2.1. These results are shown in Table 2.2.

$$2.5(O_2 + 3.76N_2) + 2H_2 \Rightarrow 2H_2O + 1.5O_2 + 9.4N_2 \tag{2.5}$$

II.3.2 PEM Fuel Cell Exhaust Condition

This section details the exhaust conditions of the PEM fuel cell cathode. These conditions are important to this investigation since variations can affect the performance of the fuel cell. Since the focus of this research is on the development of an improved moisture recovery system for PEM fuel cell applications, attention is given to those parameters which serve to affect fuel cell operation the most. Data from a parametric study (Amphlett *et al.,* 1993) was used to gage the effects of various control parameters on the PEM fuel cell performance.

Data from the study shows that there is a logarithmic increase of cell voltage relative to the ratio of increasing cell pressure to baseline pressure. Based on these results, pressurization of fuel cell reactants results in an increase in fuel cell electric output. Using the turbine side of an automotive turbocharger to extract energy from the fuel cell exhaust to power a compressor is a feasible way of increasing reactant pressure if there is a net gain.

Data from the study also revealed an increase in cell output voltage corresponding to an increase in fuel cell operating temperature. This increase does have a practical limit though. As operating temperature of the PEM fuel cell increases the resistance to exchange of protons across the membrane decreases. This is the reason for the increased electric output. The limit is due to the polymer membrane itself which is limited to operating temperatures below 80 °C.

There is also evidence from the study that excess air can increase the electric output of the fuel cell. There is a limit to this effect as well. Increasing the flow rate through the fuel cell increases the potential of dehydrating the fuel cell. An effective moisture separator could recover liquid water from the exhaust stream and use that water to maintain proper hydration of the fuel cell. But if too little water is removed from the fuel cell then the polymer membrane is flooded. Both extremes serve to lower the fuel cell efficiency.

In summary, this chapter has looked at various fuel cell types, most specifically PEM fuel cells and has developed the motivation for the choice of operating conditions for the experimental trials. Maintaining proper hydration of the fuel cell as well as meeting the reformer water requirements creates a large demand for water in the PEM fuel cell system. Water is a byproduct of the energetic reaction that occurs in the fuel cell and it is removed by means of a pressurized humid air stream. Reclaiming liquid water from the stream could increase the practicality of the PEM fuel cell in automotive applications by reducing the dependence of the system on an external water supply.

Table 2.2 Summary of Cathode Exhaust Conditions and Reformer Requirements

Cathode Exhaust Condition				Reformer Requirement
Air Mass Flow Rate	Water Vapor Mass Flow Rate	Relative Humidity	Humidity Ratio	Water Mass Flow Rate
g/min	g/min	%		g H2O/min
1930.2	223.4	100	0.1157	181.1

Chapter III

Literature Review

The literature review chapter summarizes all of the literature that was reviewed for this investigation. Review of relevant literature served not only to increase the level of understanding of fuel cell and moisture recovery fundamentals, but also to provide insight into other research with related goals. In particular, literature dealing with PEM fuel cells, moist air properties, liquid droplet formation, and centrifugal separator performance is reviewed.

III.1 Fuel Cell Fundamentals

This section details the reviewed literature that pertained to fundamentals of fuel cell operation and operating conditions.

EG&G (2002) describes the basic operating principles of fuel cells as well as different types of fuel cells available. It starts with a technology overview that describes applications and operating conditions of fuel cells currently being used. Next, advantages and disadvantages of different fuel cell types are considered along with performance characteristics of each. Finally, an overview of various fuel cell systems is provided along with a description of the type of fuel cell best suited for the use with the system based on performance data.

Hirshenhofer *et al.* (1998) presents various categories of fuel cells including PEM fuel cells. Specifics of operation including operating conditions for each type of fuel cell as well as applications are dealt with. State-of-the-art information on PEM fuel cells is provided along with a thorough discussion of PEM fuel cell reactions. In addition, hydrocarbon reformers are discussed.

McTaggert *et al.* (1998) developed an expander system for use with a 50 kW PEM fuel cell. The system employed a compressor operating in tandem with an expander to compress the air supplied to the cathode of the PEM fuel cell. The expander recovers energy from the cathode exhaust and uses that energy to power the compression process. The resulting design was a compression process aided by an electric motor. The concept of recovering energy from the cathode exhaust of a PEM fuel cell is utilized in the investigation covered by this thesis although the exact application is slightly different.

III.2 Moist Air Properties and Measurement

This section presents the reviewed literature that pertained to moisture separation and moist air property measurement.

ASHRAE (1982) provides information on standard methods for measurement of moist air properties. This literature also recommends procedures for the determination of the amount of moisture in a moving stream of air. Definitions of fundamental humidity parameters are defined and various instruments used to measure the moisture content of

air are discussed.

III.3 Centrifugal Separators

This section presents the reviewed literature that pertained to axial and tangential flow centrifugal separators.

Avci and Karagoz (1998) present a mathematical model of two phase flow in a tangential cyclone separator. Parameters that take into account geometry, surface roughness, and particle concentration are defined for the model. Several assumptions are made for the analysis, one of which is that the two phases have the same velocity and constant acceleration in the turning flow. It is also assumed that under certain conditions the drag coefficients of particles are constant. The results obtained with the assumptions are then compared to other experimental and theoretical results for different types of cyclones. The results from the model are shown to be in good agreement with observed experimental values.

Nieuwstadt and Dirkzwager (1995) outline the design of an axial flow centrifugal separator for use in applications where removal of liquid droplets from a liquid stream is desired. The primary design constraints that are considered include maximizing the swirl imparted to the stream and avoiding an adverse pressure gradient throughout the separator section. The adverse pressure gradient is shown to contribute to droplet breakup which reduces separator efficiency. An analysis of the maximum length

required for droplet removal is made that results in a swirl body geometry with a larger diameter than that of the separation zone. A stream function method is developed and presented that allows for the calculation of the flow and pressure field in this particular centrifugal geometry. Finally an example is given where it is shown that the suggested geometry does indeed avoid the adverse pressure gradient.

This literature indicates that an axial flow centrifugal separator would be preferred to a tangential flow centrifugal separator due to the large flow disturbance created by a tangential separator. Shear associated with large flow disturbances serves only to break apart the liquid droplets into smaller ones. The axial flow design minimizes the adverse pressure gradients that accompany flow disturbances and contribute to flow separation.

The implications that this literature has on separator design for a PEM fuel cell moisture recovery scheme is two-fold. First, the axial swirl element requires a smooth transition to the separation zone to aid in avoiding adverse pressure gradients. This requirement results in a swirl element with a long tail. Second, the settling length is the limiting factor for the overall length of the separator. Obviously, a smaller separator is desired. Experimental testing will be necessary to determine what effect variation in settling length has on separation efficiency.

Chapter IV

Experimental Apparatus and Instrumentation

This research aims to develop an improved system for recovering moisture from a pressurized PEM fuel cell exhaust stream using a turbocharger and moisture separator. The experimental apparatus simulated the hot and humid exhaust conditions of a PEM fuel cell and then passed that exhaust stream through the turbocharger and separator system. The experimental apparatus section gives a detailed description of the experimental test setup used in this investigation.

The first requirement of the experimental setup was to simulate the exhaust conditions of the PEM fuel cell cathode. To do so, compressed air was sent through the system and heated by an electrical resistance heater, and then it was humidified with superheated steam injected into the system from an electric boiler. The humid air stream then passed through the turbine side of an automotive turbocharger. An oil supply system was used to deliver oil to a forced lubrication journal bearing utilized by the turbocharger. As the humid air stream passed through the turbine, the temperature of the air/steam mixture dropped enough to allow liquid water droplets to condense and become entrained in the flow. The humid air stream then enters the separator as a homogeneous two phase flow. As the flow passes over the swirl element it is made to rotate strongly and the liquid droplets migrate to the wall of the separator and continue until they are subsequently removed from the flow.

In this investigation the air mass flow rate, steam mass flow rate, and heated air temperature as well as turbine inlet/outlet conditions and separator inlet/outlet conditions were measured. An array of instrumentation including Type-T thermocouples, bourdon tube pressure gages, rotameters, differential pressure transducer, and an electrical capacitance sensing relative humidity probe was used to facilitate these measurements. Readings from the thermocouples, pressure transducer and relative humidity probe were collected with a data acquisition system and subsequently logged onto a desktop computer. In addition, ambient conditions and pressure data were recorded by the researcher. Associated uncertainties for these measurements are also presented in this chapter.

The balance of this chapter is organized into sections describing the various subsystems of the experimental apparatus as follows:

1. PEM Fuel Cell Exhaust Simulation System
    - Dry Air Delivery and Heating System
    - Steam Injection System
2. Turbocharger Energy Recovery System
    - Turbine Side
    - Compressor Side
    - Oil Delivery System
3. Separator System
4. Instrumentation and Measurement Uncertainty

A schematic for the overall experimental test setup is found in Figure 4.1. Additionally, Table 4.1 and 4.2 list major components and instrumentation along with generic and commercial identification. All subsystems are mounted on a steel channel frame, specifically a Unistrut Metal Framing system chosen for its structural integrity and versatility.

Table 4.1 Experimental Apparatus Components

Description	Manufacturer	Model
Pressure Regulator	McMaster-Carr	R17-801-RGLA
Resistance Heater	Omega	FTS-048475
Flow Orifice	Gerrand Eng	¾" B-5
Steam Trap	Spirax-Sarco	B-1H
Electric Boiler	ElectroSteam	LB-20
Turbocharger	Garrett	GT-15

IV.1 PEM Fuel Cell Exhaust Simulation System

This section describes the subsystem responsible for generating the steady-state humid air exhaust stream to be passed through the turbocharger and separator systems. This system is made up of the dry air delivery and heating components and steam injection components.

IV.1.1 Dry Air Delivery and Heating System

The dry air delivery and heating system had several design requirements. First,

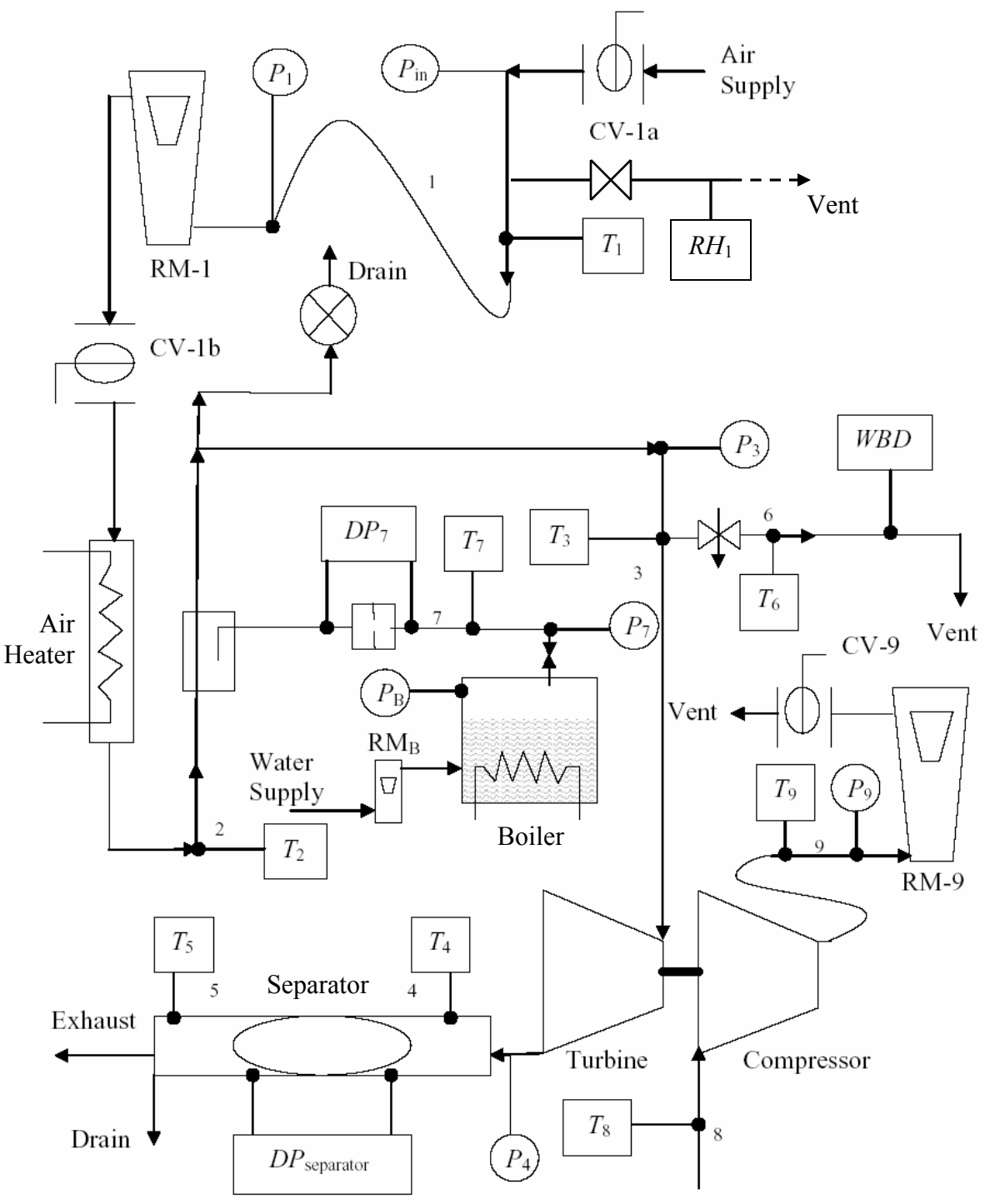

Figure 4.1 Schematic of Test Setup

Table 4.2 List of Instrumentation

Measurement	Generic Description	Commercial Description
RM_1	Rotameter	Schutte-Koerting
RM_9	Rotameter	Fischer-Porter 10A3565A
RM_B	Rotameter	Cole-Parmer N044-40
RH_1	Relative Humidity Probe	Vaisalla HMD-40
P_1	Pressure Test Gauge	Omega PGT-30L-100
P_3	Pressure Test Gauge	Omega PGT-30L-60
P_4	Pressure Test Gauge	Marshall-Town 80827
P_7	Pressure Test Gauge	Omega PGT-45B-100
P_9	Pressure Test Gauge	Omega PGT-30L-30
P_{atm}	Barometer	Swift 477
P_b	Pressure Test Gauge	Omega PGT-30L-100
ΔP_5	U-tube Manometer	Dwyer, 0 to 16 inWG, 0.2 inWG
ΔP_7	Differential Pressure Transducer	Rosemount 1151DP
T_1	Type-T Thermocouple	Omega CPSS-18U-12
T_2	Type-T Thermocouple	Omega CPSS-18U-12-DUAL
T_3	Type-T Thermocouple	Omega CPSS-18U-12
T_4	Type-T Thermocouple	Omega CPSS-18U-12-DUAL
T_5	Type-T Thermocouple	Omega CPSS-18U-12
T_6	Type-T Thermocouple	Omega CPSS-18U-12-DUAL
T_7	Type-T Thermocouple	Omega CPSS-18U-12
T_8	Type-T Thermocouple	Omega CPSS-18U-12
T_9	Type-T Thermocouple	Omega CPSS-18U-12
T_{amb}	Mercury In-Glass Thermometer	Fisher, -1 to 51 ºC, 0.1 ºC
T_{fw}	Type-T Thermocouple	Omega CPSS-18U-12
T_{oil}	Type-T Thermocouple	Omega CPSS-18U-12
WBD	Type-T Thermocouple	Omega CPSS-18U-12
m_{sep}	Mass Scale	Ohaus CT6000-S
Δt	Timer	Extech C-510

the compressed air supply was not completely dry. It contained some water vapor which would need to be reliably measured in order to determine the total amount of water that was input into the system, after the addition of steam, for the water vapor mass flow

balance. Also, the air mass flow rate needed to be accurately measured and easily adjusted in addition to being able to remain steady for extended periods of time. Next, it was required that the air be heated at constant power input so that at a steady flow rate, the air temperature is constant. It was also necessary to vary the heated air temperature prior to steam injection. Figure 4.2 shows the various components that make up the air delivery and heating system. All piping and fittings used in the air delivery and heating system are schedule 40 brass NPT unless otherwise specified. All sizes are nominal pipe sizes.

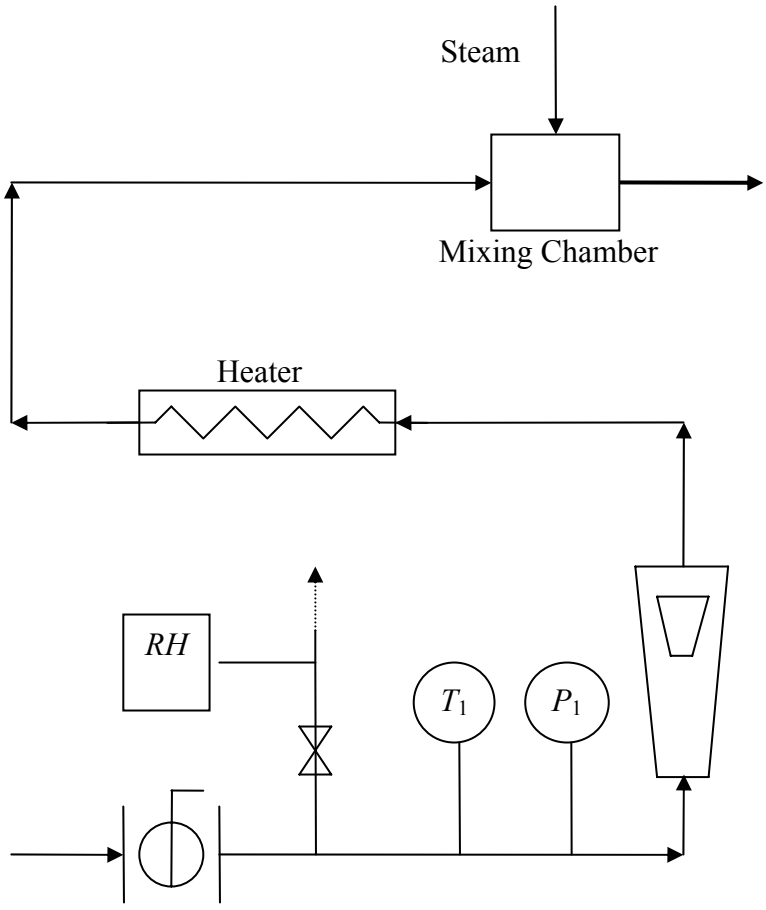

Figure 4.2 Heated Air Delivery Subsystem

The compressed air is branched from the building compressed air supply via a ¾ inch OD copper pipe, and is allowed into the system by a ¾ inch copper ball valve (CV-1a). A 1 inch internally threaded tee is connected to the ball valve by a ¾ inch pipe nipple and ¾ to 1 inch bushing. One side of the tee allows a pressure measurement (P_{in}) while the other side leads to a 1 inch pipe nipple connected to a 1 inch internally threaded tee. A thermocouple (TC-1) is threaded into one side of the tee and a 1 inch pipe nipple is on the other side which is connected to another internally threaded tee. A ¼ inch male NPT stainless steel needle valve is threaded into one side of the tee and a 1 inch CPVC tee is threaded onto the other side of CV-1b through a CPVC bushing. A relative humidity probe (RH-1) is attached to one side of the 1 inch CPVC tee perpendicular to the direction of the air flow. The other side of the 1 inch CPVC tee is left open allowing air to flow over the probe into the atmosphere. Based on the temperature (T_1) obtained from the thermocouple (TC-1) and the data from the relative humidity probe (RH-1), the moisture content of the compressed air stream can be determined.

A 1 inch flexible rubber hose attaches to the other side of the internally threaded tee that the ¼ inch male NPT stainless steel needle valve attaches to. The flexible rubber hose leads into an air pressure regulator, more specifically a McMaster-Carr R17-801-RGLA with a range of 0.135 MPa to 1.14 MPa (5 – 150 psig). The air pressure regulator has a 1 inch internal NPT thread on both the inlet and outlet. A 1 inch pipe nipple connects the outlet of the regulator to a 1 inch internally threaded tee. A pressure gage is connected to one side of the tee and a 1 inch pipe nipple connects the other side to the inlet of the air flow rotameter (RM-1). The pressure gage measures the pressure (P_1) at

the rotameter. Air mass flow rate is calculated from the compressed air inlet temperature and pressure (T_1 and P_1) and rotameter indicated float position. The rotameter has a range of 10-110 SCFM at standard conditions of 0.322 MPa (32 psig) and 21.1 °C (70 °F). At any other temperature and pressure, a correction correlation must be used to obtain the mass flow rate. A 1 inch pipe nipple is threaded into the outlet of the air flow rotameter and leads into a 1 inch nominal NPT ball valve (CV-1b). This ball valve allows the flow rate of the air to be varied and serves as the primary control of dry air into the system. Constant air mass flow rate is achieved by setting the pressure regulator and valve (CV-1b) to desired positions.

A 1 ¼ inch NPT pipe nipple is attached to the outlet of the air mass flow control valve (CV-1b) and leads into a 1 ¼ inch 90 degree internally threaded elbow. A pipe nipple connects the elbow to a 1 ¼ inch internally threaded tee. One side of the tee allows for the wiring leads of the electrical resistance air heater to pass through the system. The inlet opening is sealed to prevent air leakage. The other side of the tee leads into a 1 ¼ inch pipe nipple which connects to a 1 ¼ inch union. The union threads into a 1 ¼ inch pipe nipple. The pipe nipple serves as an enclosure for the electrical resistance air heater, more specifically an Omega Engineering model FTS-048475. The union on the inlet to the pipe nipple allows for easy access to the resistance heater. A 1 ¼ inch internally threaded tee is located on the outlet end of the heater pipe nipple enclosure. The resistance heater wiring passes through the pipe nipple enclosure and through one side of the tee. The wiring exit opening is also sealed to prevent air leakage. The other opening of the tee is the outlet passage for the compressed air after it has passed through

the heater section. A 1 ¼ pipe nipple leads from the tee to another 1 ¼ inch internally threaded tee. A dual element thermocouple (TC-2) is located in one side of the tee, and it measures the temperature (T_2) of the heated air. A 1 ¼ inch pipe nipple is threaded into the other side of the tee and leads to another 1 ¼ inch internally threaded tee. It is at this junction that the mixing of steam and dry air occurs.

The resistance air heater is a finned tube heater with a heat input range of 0 to 3.45 kW. The leads of the heater are attached to an autotransformer, more specifically a Superior Electric model 1256-b. The autotransformer allows for control of voltage across the leads of the heater which in turn controls the power dissipation or heat transfer rate to the air. One of the resistance heater elements is wired in series with a PID controller, more specifically an Omega Engineering model CN9000A. The controller receives temperature feedback from the dual element thermocouple (TC-2) measuring the heated air temperature and cuts the power if the air temperature rises above a user specified value. This controller also allows for the air to be heated to different temperatures which is a primary design parameter. The controller output signal is fed into a solid-state relay, more specifically an Omega Engineering model SSR240DC45 and switches the heater on or off. A wattmeter was used to measure the power input into the heater which is in turn the power input into the compressed air stream. The resistance heater experiences a wide temperature range during a short time span and as a result undergoes considerable thermal expansion stresses. To prevent failure associated with this phenomenon, the heater is allowed to move in the axial direction within the pipe enclosure. However, motion in the radial direction is constrained to reduced vibration induced damage.

In summary, the design requirements of the dry air delivery and heating system are as follows:

1. Measure the moisture content of the compressed air
2. Measure and adjust air mass flow rate
3. Maintain steady mass flow rate
4. Provide constant heat input to the air
5. Vary heated air temperature

The moisture content of the incoming compressed air is determined from the inlet temperature of the air and from the relative humidity measurement of the throttled air sample. The air mass flow rate is determined from inlet air temperature (T_1), pressure (P_1), and rotameter indicated position and correction. The air mass flow rate is adjusted with the air flow control valve and maintained at a steady flow rate by setting the regulator and control valve to desired positions. Constant heat input is achieved by maintaining a constant voltage across the leads of the resistance heater by means of a feedback controller. The controller also allows for variation in the heated air temperature by means of a user selectable temperature.

IV.1.2 Steam Injection System

The steam injection system had several design requirements. Primary among the requirements is that the steam injection system would add a constant mass flow of

superheated steam to the dry air flow, and it would also have to operate at steady state. The mass flow of water into the steam system and the mass flow of steam injected into the dry air stream would have to be accurately measured as well. Figure 4.3 shows the various components that make up the air delivery and heating system. The following paragraphs describe the steam injection system in detail. All pipe and pipe fittings used are brass NPT, and all sizes are nominal.

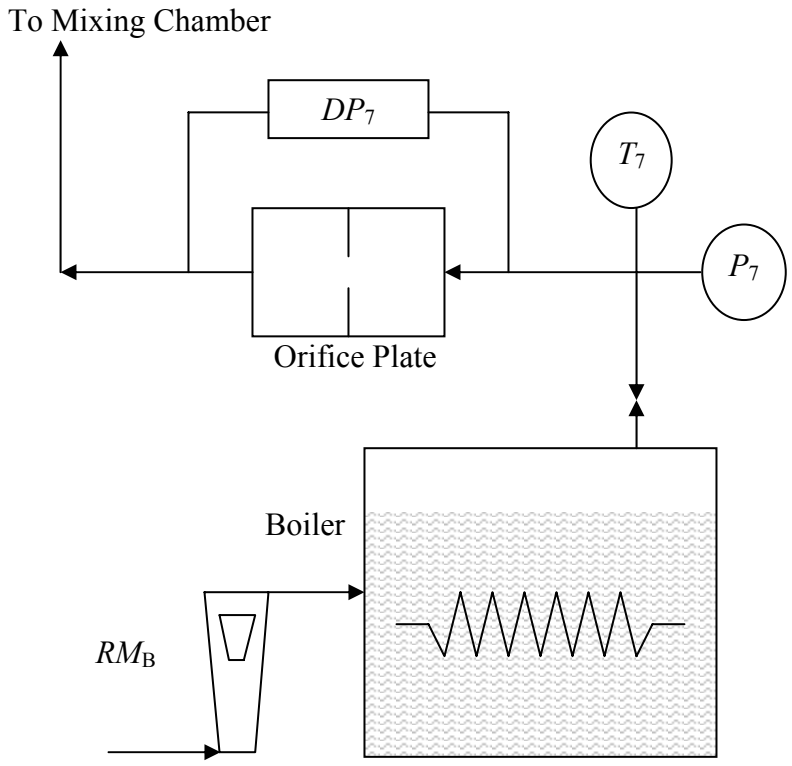

Figure 4.3 Steam Injection Subsystem

A 20 kW electric boiler, more specifically an ElectroSteam model LB-20 was used to generate the steam. The boiler used a 220 volt 3 phase electrical power supply. The building water supply was the source of water into the boiler, and the laboratory supply line was a 19 mm (0.75 inch) OD copper pipe. The supply passed through a

pressure regulator, more specifically a Honeywell model D05 before entering the boiler. Plastic tubing with an OD of 9.65 mm (0.380 inches) was attached to the outlet of the pressure regulator and carried the water to the water inlet of the boiler. A constant water level in the boiler was essential for its proper operation so a somewhat complex water delivery arrangement was used to supply water to the boiler. The system consists of a primary and secondary pump and associated piping. Figures 4.4a and 4.4b show the schematic diagram and picture of the boiler water supply arrangement. The primary water supply pump is a Teel model 4P919. This pump operates continuously during steam generation. The secondary pump is a Teel model 3P714 and functions as an emergency backup pump to prevent the boiler from operating dry. The secondary pump would only be activated when the low level switch on the boiler was triggered. Both pumps are rotary vane pumps with internal bypass.

The water enters the boiler supply on one side of a ¼ inch tee. The tee splits the inlet water flow between the primary and secondary pumps. The outlet of the tee that leads to the primary pump is connected to a ¼ inch nominal ball valve (CV-7e). Plastic tubing with an OD of 9.65 mm (0.38 inch) directs the flow from the ball valve to the primary pump. A ¼ inch pipe nipple connects the outlet of the pump to a ¼ inch internally threaded cross. One side of the cross is fitted with a brass needle valve (CV-7f). The purpose of the needle valve is to control the flow of water diverted from the boiler to the laboratory drain. Another side of the cross is fitted with a thermocouple (TC-feedwater) that measures the boiler inlet water temperature. The final side of the cross allows the water to exit through a ¼ inch pipe nipple which leads into the boiler

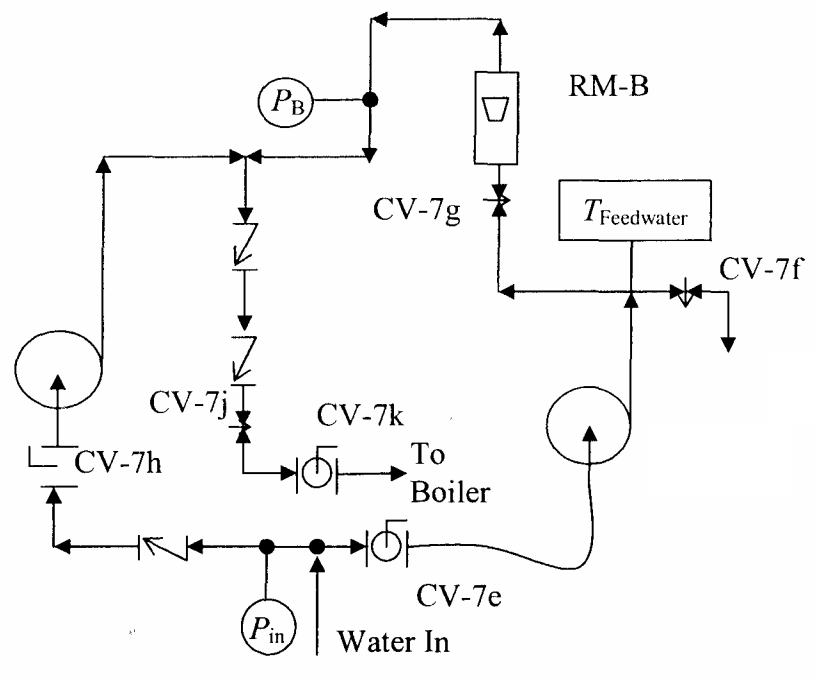

Figure 4.4a Schematic of Boiler Water Supply

inlet rotameter (RM-B). The boiler rotameter serves two purposes. It allows the water flow into the boiler to be measured and controlled. A needle valve (CV-7g) on the inlet side of the rotameter allows for adjustment of the flow. The outlet of the rotameter leads into a ¼ inch pipe nipple which directs the water to an internally threaded tee. One side of the tee is fitted with a pressure gage where a pressure measurement (P_B) is taken. The other side of the tee leads through a series of ¼ inch 90 elbows and pipe nipples to direct the flow to the main boiler feed line ½ inch tee. One side of this tee leads to the secondary pump inlet and the other side leads to the main boiler feed line outlet.

The other side of the ¼ inch tee on the boiler supply inlet leads to the secondary pump. Inline is a pressure gage where a pressure (P_{in}) is measured. The inlet water pressure gage insures that the pump supplying water to the boiler has pressure at all times

during operation. An electrically actuated (CV-7h) valve follows the pressure measurement. This valve is triggered by the low level switch on the boiler and only opens in a low level situation. When the low level switch is triggered the secondary pump is also activated. After the electrically actuated valve is another series of ¼ inch 90 degree elbows and nipples that direct the flow to the secondary pump inlet. The discharge side of the secondary pump leads into the main boiler feed line ½ inch tee described above.

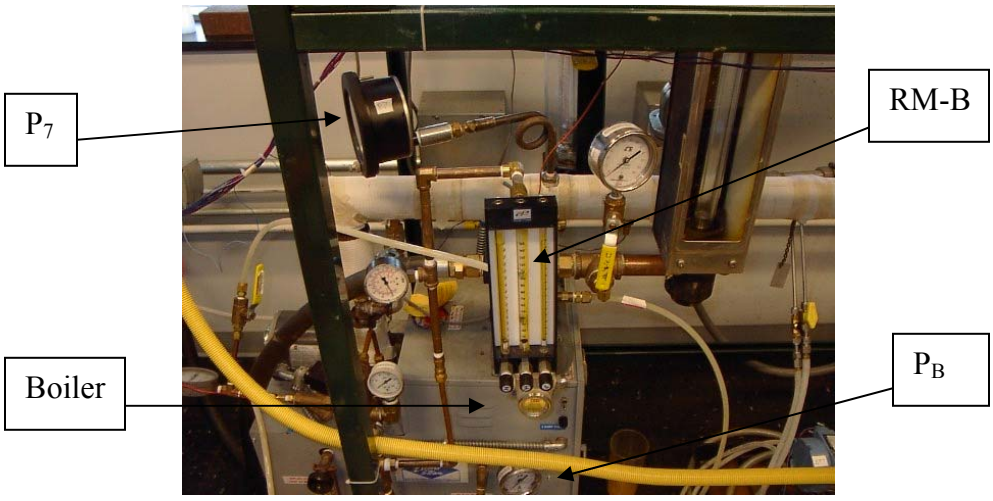

Figure 4.4b Picture of Steam Boiler and Instrumentation

The primary and secondary pump discharge lines meet at two sides of the main boiler feed line ½ inch tee. The other side of the tee leads to a ½ inch pipe nipple which leads into two inline ½ inch spring loaded check valves. The check valves prevent any backflow into the primary and secondary pump loops. The check valves lead into a ½ inch pipe nipple and then into a ½ inch 90 degree elbow. The elbow exits into a ½ inch internally threaded ball valve (CV-7j) which leads into a ½ inch pipe nipple terminating

in the boiler tank.

The boiler produces superheated steam to the boiler exit which is throttled through a ½ inch nominal brass ball valve (CV-7a). The superheated steam exits the valve and flows through a ½ inch pipe nipple and on through a ½ inch 90 degree elbow. The elbow directs the flow into a gate valve (CV-7b) and then the flow expands into a ¾ inch stainless steel pipe nipple which leads to a ¾ inch tee. The gate valve is available for bypassing the system and allowing some amount of the steam to vent into the atmosphere but it was not used for this experiment however. One side of the tee is fitted with a pressure gage which measures the superheated steam pressure (P_7) after the boiler. The other side of the tee leads to another ¾ tee with one side fitted with a thermocouple (TC-7). The other side of the tee directs the flow through a ¾ inch pipe nipple leading into a brass corner tapped flow orifice or more specifically Gerrand Engineering model ¾ inch B-5. On either side of the orifice plate are pressure taps which are connected to a differential pressure transducer (DP-7). The mass flow rate of steam is calculated from the temperature (T_7) and pressure (P_7) of the superheated steam as well as the differential pressure across the orifice.

Following the orifice flow plate is a ¾ inch pipe nipple that leads to a ¾ inch tee. One exit of the tee is facing downward while the other exit faces upward. The downward facing end is fitted with a ¼ inch stainless steel needle valve which functions as a steam trap allowing condensate to escape while minimizing steam loss. The upward facing end leads into a ¾ inch pipe nipple connected to a ½ inch brass ball valve (CV-7d). This

valve serves as the primary control of steam injected into the system. The ball valve exits into ½ inch copper pipe that directs the flow into the injection chamber which is a 1 ¼ inch tee. A 60 degree full cone steam nozzle or more specifically a McMaster-Carr item 32885K58 is attached to the end of the copper tube and serves as the injector for the steam into the chamber. The chamber allows the dry air stream and superheated steam stream to be well mixed.

All piping and fittings between the steam injection chamber and the inlet side to the turbine are schedule 40 brass and nominal NPT sizes. After the injection chamber, the mixture flows into a 1 ¼ inch pipe nipple and then into a 1 ¼ inch tee. One side of the tee is fitting with a ½ inch reducing bushing that leads into a steam trap, more specifically a Spirax-Sarco model B-1H. The steam trap allows for the exit of any condensate that has formed while preventing escape of the pressurized mixture. The other end of the tee changes the direction of the flow by 90 degrees and routes it into another 1 ¼ inch tee. One of the ends of the tee is fitted with a pressure gage where a pressure (P_3) is taken. The flow is then routed through another 90 degree turn out of the remaining end of the tee into a 1 ¼ inch cross. One of the 90 degree oriented ends of the cross is fitted with a thermocouple (TC-3) where the mixture temperature (T_3) is taken. The other 90 degree oriented end is fitted with a ½ inch male needle valve (CV-6) that allows the mixture to be throttled to atmospheric pressure for the purpose of making a wet and dry bulb temperature measurement. The remaining end of the cross directs the flow into the turbine side of the turbocharger.

The humidity ratio of the mixture is necessary for determination of the amount of liquid that will be available for separation after the turbocharger. Wet and dry bulb temperatures allow for the calculation of the humidity ratio and are measured directly. The dry bulb temperature is measured with a thermocouple (TC-6) and the wet bulb temperature is measured by a thermocouple (TC-WBD) covered with a wetted wick. The dry bulb temperature measurement is rather straightforward as it consists of a single thermocouple measurement. The wet bulb measurement however is inherently delicate. First, the pressurized stream has to be throttled down to atmospheric pressure so the throttling valve requires a setting that allows the drop to atmospheric pressure without a substantial loss of the pressurized stream. Another complicating feature of the wet bulb measurement arises from the wetted wick that is placed over the thermocouple junction. If the wick is not fully saturated or dries out, then the temperature measured will be identical to the dry bulb temperature. If the wick becomes oversaturated then the temperature measured will be that of the water used to hydrate the wick.

The following setup was utilized to facilitate an accurate wet and dry bulb measurement. After the pressurized stream is throttled through the ½ inch needle valve (CV-6), it flows through a ½ inch 90 degree elbow. The flow is directed from the elbow through a ¼ inch tee where a thermocouple (TC-6) is fitted for the dry bulb temperature measurement. The flow passes through the tee and exits into a ¼ inch cross. One end of the cross is oriented down and is fitted with a 12.7 mm (0.5 inch) OD clear rubber tube that attaches to the bottom of a clear cylindrical water reservoir which is filled with distilled water. Another end of the cross is fitted with a welded thermocouple wire that is

placed into the throttled stream. The thermocouple junction is jacketed by a cotton wick which extends down through the rubber tube and into the water reservoir. Capillary forces draw water to the top of the wick to keep the thermocouple junction saturated. Figure 4.5 shows the wet and dry bulb temperature measurement is schematic setup. A delta temperature configuration was used in the thermocouples to make the wet and dry bulb temperature measurements. The thermocouple (TC-6) used for the dry bulb temperature measurement is a dual element thermocouple. One element is connected in series with the thermocouple used to make the wet bulb depression measurement. The voltage read from the dry bulb temperature thermocouple was correlated directly to temperature. The differential voltage read at the wet bulb depression terminals was correlated to temperature using the Sebeck coefficient for a Type T thermocouple. This investigation used a Sebeck coefficient of 4.3×10^{-5} V/°C corresponding to a constant temperature of 60 °C. Due to inconsistent readings arising from the difficulty in monitoring and maintaining proper wick hydration however, the orifice flow meter was relied upon as the primary means of measuring the steam mass flow rate.

In summary, the design requirements of the steam injection system are as follows:

1. Add constant mass flow of superheated steam to the dry air stream
2. Operate at steady state
3. Accurately measure the mass flow rate of steam into the dry air stream and associated properties

The steam injection system maintains a constant flow rate of steam by means of a

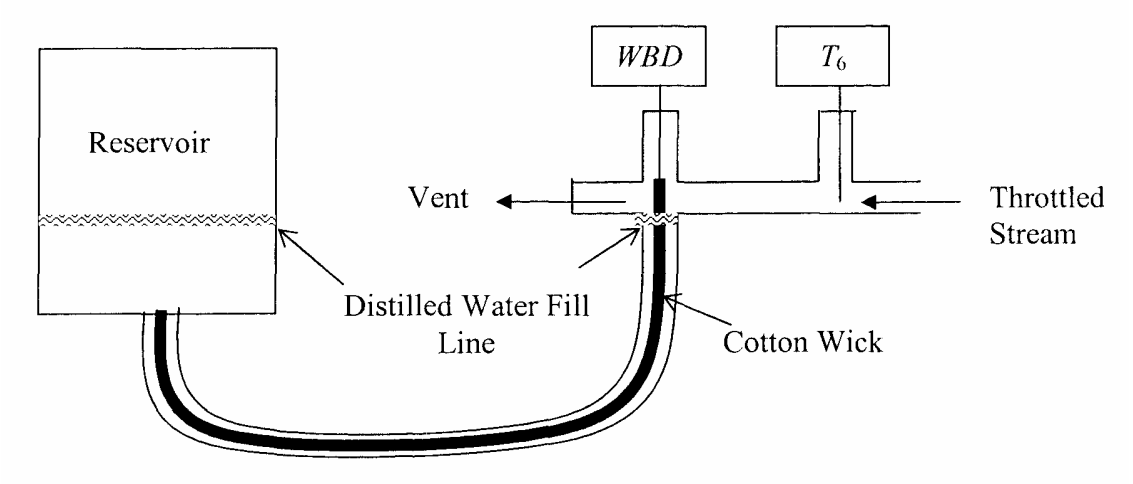

Figure 4.5 Schematic of Wet-Bulb Measurement Setup

somewhat complicated arrangement of pumps, valves and piping. A boiler rotameter and orifice flow meter as well as carefully instrumented thermocouples and pressure gages allow for accurate measure of the steam flow rate at steady state operation.

IV.2 Turbocharger Energy Recovery System

The turbocharger subsystem section details the part of the experimental setup involving the turbine and compressor sections of the turbocharger. The turbocharger energy recovery system is comprised of the turbine, compressor, and oil delivery subsystems which are described in detail below. Figure 4.6 shows a picture of the turbocharger used in this apparatus.

IV.2.1 Turbine Side

After the dry air stream is injected with steam, the mixed stream expands through the

turbine side of an automotive turbocharger. The result is a drop in both temperature and pressure of the stream and formation of liquid water condensate in the stream. The purpose of the turbine is to recover energy from the humid stream by converting it to shaft work while condensing liquid water out of the stream. The turbine side is instrumented to measure power output from the turbine. Figure 4.1 shows the turbine side of the turbocharger as well as instrumentation in schematic form. All pipe and fittings are brass with NPT threading unless specified otherwise and all sizes are nominal.

The humid air stream is expanded through the turbine side of an automotive turbocharger specifically a Garret model GT-1541V. The flow is directed out of the turbine by a 1 ¼ inch pipe nipple and leads to a 1 ¼ inch tee. One side of the tee is fitted with a pressure gage for measuring the turbine outlet pressure (T_4). The turbine exhaust passes through the remaining opening via a 1 ¼ inch pipe nipple. The other end of the pipe nipple is threaded with a 1 ¼ PVC union that couples to the inlet pipe of the separator.

IV.2.2 Compressor Side

The compressor side of the turbocharger utilizes the shaft power output from the turbine to compress ambient air. The compressor system is instrumented to obtain data for power calculations. Figure 4.1 shows the compressor side of the turbocharger as well as instrumentation in schematic form. All piping has NPT threading unless specified otherwise and all sizes are nominal.

The compressor side of the turbocharger draws in ambient room air for compression which makes it susceptible to damage from foreign particles in the atmosphere that are entrained in the inlet flow. Therefore a filter, more specifically a Mc-Master-Carr model 4399K45, is used on the compressor inlet. The filter is connected

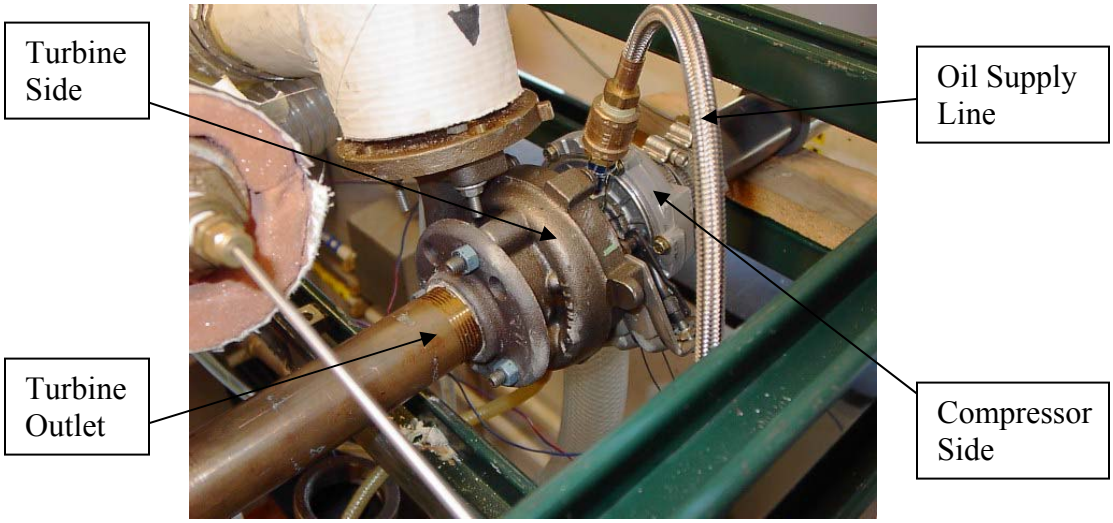

Figure 4.6 Turbocharger Energy Recovery System

to a 1 ½ inch PVC pipe nipple that leads to a 1 ½ inch flexible pipe coupling. The coupling is secured to the compressor inlet with pipe clamps. A thermocouple (TC-8) is inserted into a fitting that is threaded into the 1 ½ inch PVC pipe nipple for measurement of compressor inlet air temperature (T_8). The air is compressed and then exits through a clear flexible reinforced rubber hose. The hose is attached to the compressor exit with a pipe clamp. A thermocouple (TC-9) is inserted into the rubber hose near the compressor exit to measure the compressor exit temperature (T_9). The rubber hose leads into 1 ½ inch stainless steel pipe nipple which leads to a 1 ½ inch stainless steel tee. The tee is fitted with a pressure gage to measure the compressor outlet pressure (P_9). The tee then

attaches to the inlet of a rotameter (RM-9) specifically a Fischer-Porter model 10A3565A. The rotameter measures the mass flow rate of air through the compressor. A 1 ½ inch nominal ball valve (CV-9) is attached to the outlet of the rotameter and allows the flow through the compressor to be throttled. The outlet of the valve directs the flow into the atmosphere.

IV.2.3 Oil Delivery System

The turbocharger used in this investigation was designed for automotive use and required a continuous oil feed to its forced lubrication journal bearing. An oil delivery loop was utilized for this purpose. The manufacturer recommended SAE 10W-30 motor oil supplied at a pressure between 1.7 and 5 bar (24.7 and 72.5 psig) and exiting at atmospheric pressure. The recommended temperature range is between 38 and 130 °C (100 and 266 °F). Figures 4.7 shows the oil delivery system in more detail and Table 4.3 lists the generic and commercial identification of individual components. All pipe and fittings are brass and are nominally sized with NPT thread sizes. The oil pump specifically a Hypro model 0503C-DE is gravity fed from a 2 inch galvanized pipe that acts as an oil reservoir. The oil is fed into the pump from the reservoir through a reduction connected to a ½ pipe nipple and ½ inch union. The oil leaves the discharge side of the pump through a ½ inch pipe nipple. A ½ inch tee is connected to the pipe nipple. The other side of the tee leads to an oil filter. The oil leaves the filter through a ½ inch pipe nipple and is turned vertically through a ½ inch 90 degree elbow. A ½ inch pipe nipple connected to the elbow and leads into a ½ inch cross. One side of the cross is

fitted with a thermocouple (TC-oil) to measure the oil temperature. The pump used to supply oil delivers approximately 13.2 liters per minute (3.5 gpm) at a pressure of 3.1 bar (30 psig). Since only a portion of this volume is required by the bearing, a bypass valve is used to divert some of the oil. The bypass valve is located on the cross opposite of the thermocouple. The valve diverts some of the oil back to the reservoir through a piece of ½ inch copper tubing. The remaining outlet on the cross leads to a ½ inch nipple which

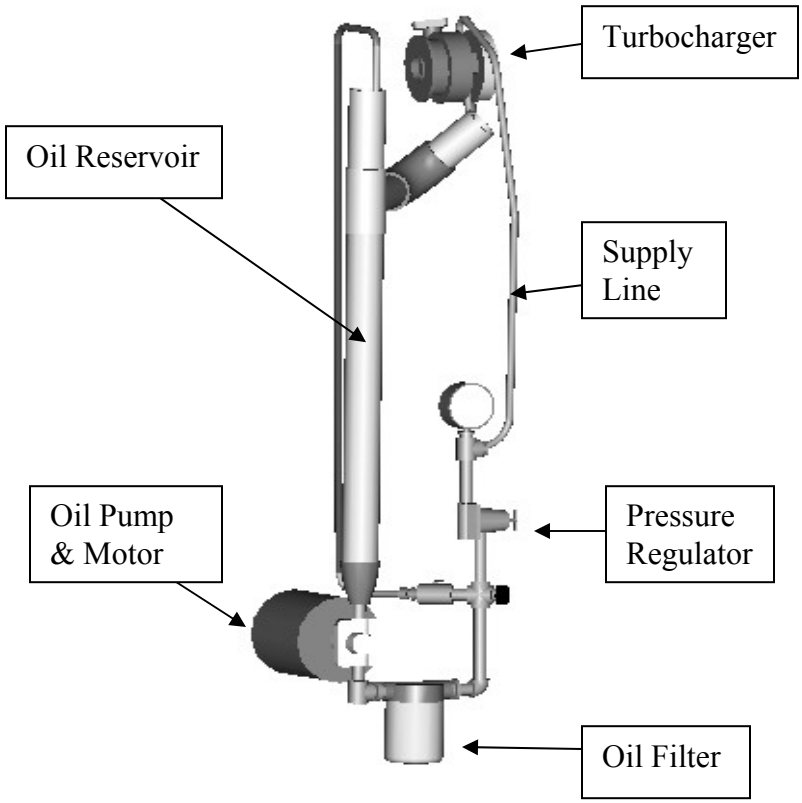

Figure 4.7 Oil Delivery System

directs the flow to a pressure regulator, specifically a Watts model 2A65. The regulator is set to maintain the oil pressure at 3.1 bar (30 psig). The oil leaves the regulator through a ½ inch tee and is directed through a ½ inch tee. One side of the tee is fitted with a pressure gage for measuring oil pressure (P_{oil}). The other side is fitted with a

flexible metal hose that delivers the oil into the turbocharger oil inlet passage. The oil exits the turbocharger at atmospheric pressure through a flexible reinforced rubber hose and returns to the oil reservoir.

In summary, the turbocharger energy recovery system is comprised of a turbine side and compressor side of the turbocharger in addition to the oil delivery system. The turbine extracts energy from the pressurized humid air stream and converts it into shaft work to drive the compressor. The expansion through the turbine also results in the formation of condensate due to the corresponding pressure and temperature drop of the humid stream.

IV.3 Moisture Separator

This section describes the part of the experimental setup involving the axial flow moisture separator. The primary design requirement of the separator system was to remove liquid water from the humid stream without causing a large pressure drop through the separator section. Figure 4.8 shows the separator in schematic form. Chapter V gives more detail on the design methodology used to develop the separator as well as information on the actual construction of the swirl element and separator housing. The separator section removes the liquid condensate from the humid stream that forms as a result of expansion through the turbine side of the turbocharger. Once the liquid is removed, the stream leaves the separator and is directed outside into the atmosphere. The separator is instrumented to allow for measurement of temperature into and out of the

separator as well as pressure drop across the swirl element.

IV.4 Instrumentation and Uncertainty

In this investigation the air mass flow rate, steam mass flow rate, and turbine inlet/outlet conditions and separator inlet/outlet conditions were measured in order to characterize the performance of the separator. In addition, there were several other temperature and pressure measurements made to insure the proper operation and safety of the experimental apparatus. An array of instrumentation including thermocouples, pressure gages, rotameters, pressure transducer, and relative humidity probe were used to facilitate these measurements. Readings from the thermocouples, pressure transducer and relative humidity probe were collected with a data acquisition system and subsequently logged onto a desktop computer. Ambient conditions as well as pressure data were recorded by the researcher. This section identifies all instruments used as well as associated uncertainties for these measurements.

The data acquisition system used for this experiment consisted of an Agilent model 34970A and HP Data Logger software. A personal computer running the Windows 95 OS was used to collect, store, and process data. The acquisition card had twenty voltage slots and 2 current slots available for measurement. Twelve voltage slots were used for thermocouple measurements while both current slots were used for the orifice differential pressure measurement and relative humidity measurement. Correction coefficients obtained through individual calibrations were input directly into the data

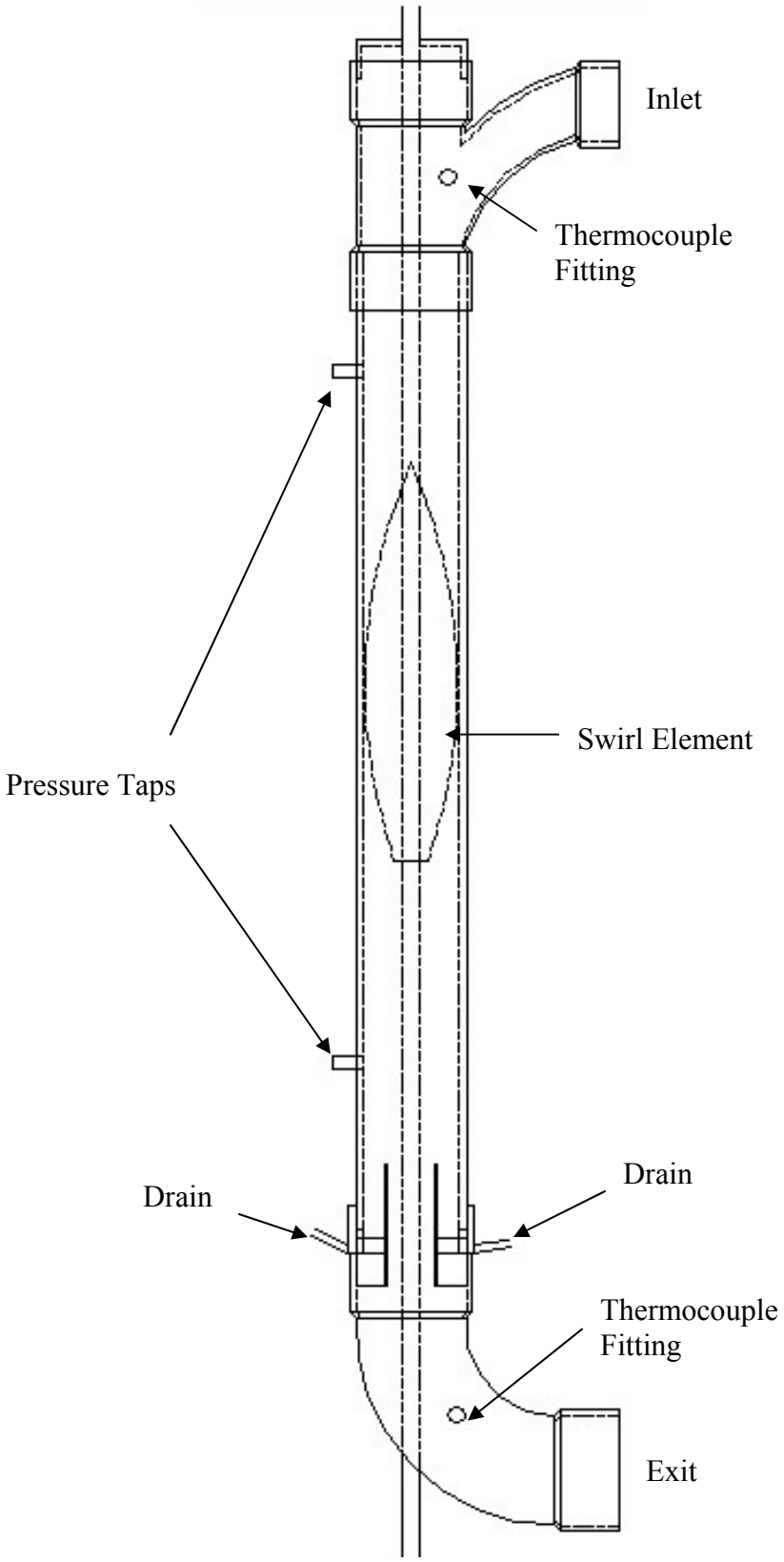

Figure 4.8 Schematic of Moisture Separator

logging software. All data collected were integrated over 20 power line cycles. Table 4.2 lists all of the measurement instrumentation used in the experimental apparatus.

All thermocouples were calibrated prior to the experimental trial runs. The thermocouples were calibrated six at a time by immersion in a constant temperature bath, specifically a Techne Block Calibrator model DB-35L. Glycerin was used as the bath fluid and an RTD, more specifically an Omega model PRP-2, was used as the temperature standard. The resistance of the RTD was read by a digital multimeter, more specifically a Hewlett Packard model 34401A, which was set up for a four-wire resistance measurement. The data acquisition system was set up to display the output for a standard T-type thermocouple with zero offset and a gain of one. The temperatures measured by the RTD were plotted against those measured by the thermocouples. A linear regression was performed and the correction coefficients were obtained for each thermocouple. Equation 4.1 shows the general form for the regressions.

$$T_{corr} = mT_{meas} + b \tag{4.1}$$

Where: T_{corr} is the corrected temperature

T_{meas} is the temperature read by the thermocouple

m is the slope from the regression (gain)

b is the intercept from the regression (offset)

The gain and the offset were input directly into the data logging software which displays

corrected temperatures. Regression results can be found in Appendix A.

A calibration was also performed for the boiler feedwater rotameter by using the weighing tank method. For the calibration, the outlet of the rotameter was diverted into a weighing tank situated on a mass scale, specifically an Ohaus model CT6000-S. Water was allowed to flow through the rotameter into the weighing tank and the corresponding elapsed time was measured. The mass flow rate was then plotted against the rotameter reading. A regression similar to that performed on the thermocouples was then performed for the boiler rotameter. The regression result provides the *m* and *b* coefficients for the boiler rotameter. Those results are found in Appendix A.

The orifice flow differential pressure transducer (dP-7) requires a 12 to 45 V DC power supply and provides a 4 to 20 mA output. Calibration data obtained during a previous phase of this project was used for the transducer. This information can be found in Appendix A.

The turbocharger is also instrumented with an optical tachometer to measure the rotational speed of the compressor shaft. Table 4.3 lists the components that make up the tachometer. The transducer emits a visible red light which is carried through one cable into the lens. The lens is embedded into a hole which was drilled into the compressor casing. The hole maintains the focus of the light at a normal orientation onto the shaft. Half of the circumference of the shaft is non-reflective while the other half is reflective. When the red light reflects from the shaft, it is detected by the transducer which generates

an electric signal. When the red light is not reflected, an open circuit condition is created and the transducer outputs no signal. The electric signal is counted by a counter, specifically a Hewlett-Packard 5314 A. The pulse count represents the rotational speed of the compressor shaft.

Table 4.3 Optical Tachometer Components

Generic Identification	Commercial Identification
Transducer	Banner D12SN6FPYQ
Fiber Optic Cable	Banner PBCT26U
Lens	Banner L4C20

IV.4.1 Uncertainty Due to Precision Error

Uncertainty due to precision error, denoted as U_A, is a measure of the random deviation in a measurement. U_A can be addressed through statistical means as it represents the deviation of repeated measurements from the average of the repeated measurements.

All temperature measurements, excluding ambient temperature, along with the compressed air relative humidity, wet-bulb depression, and orifice differential pressure measurements were collected with a digital data acquisition system. Even while operating at steady state, the readings for each measurement showed some random variation. U_A for the digital measurements in this investigation was estimated by recording several successive values while operating at a steady state and performing a statistical analysis. For each measurement Equation 4.2 was used to estimate U_A.

$$U_A = k_c \frac{\sigma}{\sqrt{n}} \tag{4.2}$$

where

σ = standard deviation of the sample

n = number of data points in the sample

k_c = coverage factor based on statistical degrees of freedom and 95% confidence interval

The data in Table 4.4 will be used as an example. In the example, there are 10 successive measurements. The standard deviation of the sample is 0.020 ºC. The coverage factor determined from a t-distribution with a 95% confidence interval and 9 degrees of freedom is 2.26. The resulting U_A is 0.014 ºC. The U_A for all equipment having digital readings is shown in table 4.5.

The U_A for analog instruments such as pressure gages and rotameters can be addressed by evaluation of resolution limitations. In general, the U_A is taken to be one half of the finest graduation. U_A for the analog instruments can also be found in Table 4.5.

IV.4.2 Uncertainty Due to Possible Bias

Uncertainty due to possible bias, denoted by U_B, is often a symptom of inadequate calibration. All of the thermocouples used were calibrated prior to any experimental trials. All of the calibrations performed for this experiment resulted in a linear regression

model. The expanded error due to possible bias, or U_B, was determined from the Standard Error of Estimate (SEE) which resulted from the linear regression models. Table 4.5 list the U_B data obtained for each of the thermocouples.

A calibration similar to that performed on the thermocouples was performed for the boiler rotameter and a linear regression model was generated. Once again, the uncertainty due to possible bias for the rotameter was determined from the Standard Error of Estimate (SEE) that resulted from the linear regression model. The resulting U_B from the rotameter calibration is shown in Table 4.5.

Table 4.4 Sample Data Used for Determination of U_A for TC-1

	T_1
	ºC
1	20.775
2	20.751
3	20.757
4	20.745
5	20.749
6	20.707
7	20.719
8	20.735
9	20.752
10	20.730
average =	20.742
st. dev. =	0.020
k_c =	2.262
U_A =	0.014

Uncertainty due to possible bias for each of the pressure gauges and relative humidity meter was determined from manufacturer's stated total uncertainty. These

values are displayed in Table 4.5. The U_B for the orifice differential pressure transducer was determined from calibration data collected during a previous phase of the experiment. This data can be found in Appendix A. The SEE from the resulting linear regression model was used to determine the U_B for the differential pressure measurement. The U_B for the manometer used to measure the pressure drop across the separator was shown to be negligible due to zeroing.

Table 4.5 shows U_A and U_B data for the instrumentation used in this investigation. This table also includes the combined uncertainty for the instrumentation for convenience. The combined uncertainty is computed with Equation 4.3

$$U_A^2 + U_B^2 = U_C^2 \tag{4.3}$$

In summary this section provides a description of the various instruments utilized for this investigation and describes the various calibrations which were performed. It also provides estimates for uncertainty due to precision error as data pertaining to error to possible bias.

Table 4.5 Uncertainty Due to Precision and Bias Error for Instrumentation

Measurement	U_A	U_B	U_C
RM_1	1 scfm	N/A	1 scfm
RM_B	0.5 mm or 2 ml/min	4.5 ml/min	4.9 ml/min
RH_1	0.001%	0.003%	0.003%
P_1	0.25 psi	0.5 psi	0.56 psi
P_3	0.1 psi	0.3 psi	0.32 psi
P_4	0.5 mm Hg	0.5 mm Hg	0.71 mm Hg
P_7	0.25 psi	0.25 psi	0.35 psi
P_9	0.1 psi	0.15 psi	0.18 psi
P_{atm}	5 mm Hg	N/A	5 mm Hg
P_B	0.25 psi	0.5 psi	0.56 psi
ΔP_5	0.1 in. H_2O	negligible	0.1 in. H_2O
ΔP_7	0.024 in. H_2O	0.092 in. H_2O	0.094 in. H_2O
T_1	0.014 ºC	0.22 ºC	0.38 ºC
T_2	0.011 ºC	0.40 ºC	0.22 ºC
T_3	0.008 ºC	0.08 ºC	0.11 ºC
T_4	0.015 ºC	0.05 ºC	0.05 ºC
T_5	0.034 ºC	0.15 ºC	0.11 ºC
T_6	0.012 ºC	0.10 ºC	0.27 ºC
T_7	0.027 ºC	0.44 ºC	0.058 ºC
T_8	0.030 ºC	0.08 ºC	0.78 ºC
T_9	0.030 ºC	0.22 ºC	0.73 ºC
T_{amb}	0.050 ºC	0.05 ºC	0.05 ºC
T_{fw}	0.010 ºC	0.05 ºC	0.041 ºC
T_{oil}	0.014 ºC	0.18 ºC	0.014 ºC
WBD	0.018 ºC	N/A	0.018 ºC
m_{sep}	1 g	N/A	1 g
Δt	0.01 s	N/A	0.01 s

Chapter V

Experimental Procedure

The experimental procedure section details the steps taken during the experimental trials used to evaluate the performance of the moisture separator. The purpose of the experimental procedure is to insure that the results of this investigation are reliable and repeatable. Consistent execution of the experimental procedure insures that the data was collected at steady state operation.

Some steps that are part of the procedure were included to insure operator and system safety. For the personal safety of the operator, eye and hearing protection were required at all times during experimental trials. There were also several requirements for the safe operation of the experimental apparatus. It was necessary for the oil pump to be in operation any time that air was flowing through the system to protect the main bearing in the turbocharger. Similarly, it was necessary for air to be flowing through the system any time the resistance heater was in operation. Not doing so could allow overheating which could damage heater components. The steam boiler also presented another possible hazard due to the threat of steam entering the unpressurized system after the air flow was shut off. Steam entering the system without air flow could potentially flow back into the resistance heater section and condense onto electrical connections. The presence of water in that area could result in damage caused by electrical short circuits. This problem is avoided by closing the primary and secondary steam control valves during the shutdown procedure.

It was necessary for the experimental apparatus to operate in steady state in order to obtain accurate data. The data acquisition system that was used in this experiment constantly logged data from startup throughout shutdown. Measurement values for thermocouples, humidity probe, and orifice flow meter were displayed for each interval in the logging sequence. In addition, graphical presentation of the data in the form of strip charts were displayed for oil temperature, heated air temperature, steam temperature, mixture temperature and turbine inlet/outlet temperatures allowing for a quick check of system parameters. The system was considered to be at steady state when the temperature readings changed no more than 0.1 °C during a 5 minute span.

Once steady state operation was obtained, outside demand on water and air supply could cause an imbalance in the system and disrupt the steady state operation. Fluctuations in water pressure affect the flow of water into the boiler which directly affects the steam mass flow rate out of the boiler. To prevent the fluctuations, a regulator was used to restrict the water pressure to 3 bar (30 psig) from the 4.1 bar (45 psig) of the building supply. It was also important to monitor the boiler operation as well. A watchglass was available on to the boiler to indicate the water level. At steady state operation, this level was constant. In addition to the water level, boiler pressure was monitored along with orifice differential pressure. Inlet flow was adjusted with the boiler rotameter until the orifice pressure drop changed no less than 0.05 in. H_2O over a five minute period. The inlet air pressure was also prone to the same type of fluctuations as the boiler water supply. Again, a pressure regulator was employed to maintain the air pressure at a steady value.

The following steps were taken during each experimental trial. Figures 4.1, 4.2b and 4.5 show the overall experimental apparatus, boiler water supply, and oil delivery subsystem respectively.

1. The data acquisition system was initialized along with the DC power supplies for the humidity probe, orifice differential pressure transducer, and tachometer.
2. The oil bypass valve was set to the fully open position.
3. The oil delivery pump for the turbocharger and wattmeter were energized.
4. Once the oil temperature reached 38 °C (100 °F), the oil bypass valve was closed until the oil pressure reached 3.1 bar (30 psig). The oil pressure regulator was set at 3.1 bar (30 psig) following the turbocharger manufacturer recommendation.
5. The air inlet ball valve (CV-1a) was set to the fully open position.
6. The air heater main power switch was flipped, and the air heater was energized. The autotransformer was adjusted to 0.75 kW and the heated air temperature was set.
7. The three phase main power switch for the boiler was flipped, and the boiler was energized.
8. Once the boiler pressure reached 5.9 bar (70 psig), the primary boiler ball valve (CV-7a) was set to the fully open position.
9. The boiler steam trap needle valve (CV-7c) was opened to allow condensed steam to exit the supply line. It was then closed partially to allow condensed

steam to exit while minimizing steam loss.

10. The boiler secondary ball valve (CV-7d) was partially opened to allow steam to be injected into the system.
11. The primary boiler pump was energized with a 110 VAC power source.
12. The boiler rotameter valve (CV-7g) was adjusted in tandem with the boiler secondary ball valve (CV-7d) until steady state steam flow was achieved. Steady state operation was reached when the water level in the boiler watchglass was constant and the orifice differential pressure changed by no more than 0.05 in. H_2O over a five minute period.
13. Distilled water was added to the wet bulb reservoir and the wet bulb throttling valve (CV-6) was opened fully to allow the wick to become saturated. The valve was then partially shut to facilitate the wet bulb measurement.
14. The system was allowed to run so that all measurements reached steady state values.
15. The condensation from the boiler steam trap over a five minute period was collected and measured.
16. All steady state temperatures, pressures, and flow rates as well as air relative humidity were recorded.
17. The moisture recovery container was placed under the separator while simultaneously starting the stopwatch.
18. The moisture recovery container was allowed to fill and then it was removed while simultaneously stopping the stopwatch.
19. The data was then input in the EES program to check for any anomalies

before changing settings.

20. The heated air temperature was adjusted and steps 14 through 19 were repeated each trial.
21. All data logged during the session were then saved to the computer hard drive.
22. The boiler was de-energized and the primary and secondary boiler valves were set fully open to relieve boiler pressure.
23. Once boiler pressure reached approximately 3 bar (30 psig), the primary and secondary boiler ball valves were set fully closed.
24. The primary boiler pump was shut off once the boiler watchglass showed that the boiler water level was full.
25. The heated air was allowed to run through the system for 2 minutes and then de-energized.
26. Once the air temperature dropped below 30 °C (86 °F) the air inlet ball valve (CV-1a) was set fully shut.
27. The oil bypass valve was set fully open and the pump was de-energized.
28. All DC power supplies were shut off and the data acquisition system was deactivated.

Experimental trials were carried out for three different positions of the swirl element in the separator housing. Data were collected with the swirl element placed near the inlet to the separator housing and near the exit. Additionally, data was collected with the swirl element placed at a midrange position. The various positions permitted the evaluation of design performance for the maximum settling length allowed by the separator housing

and for the design settling length of 30 cm (12 in.) as well as a midrange settling length of 46 cm (18 in.). Table 5.1 lists all data that was collected for processing during the experimental trials. Uncertainty data for these measurements are presented in Section IV.4.

Table 5.1 Listing of Data Collected for Processing During Experimental Trials

Measurement	Description
RM_1	Inlet Air Flow Rate
RM_B	Boiler Feedwater Flow Rate
RH_1	Relative Humidity of Inlet Air
P_1	Inlet Air Pressure
P_3	Turbine Inlet Pressure
P_4	Turbine Outlet Pressure
P_7	Steam Pressure Upstream of Orifice
P_{atm}	Ambient Air Pressure
P_B	Boiler Pressure
ΔP_5	Pressure Drop across Separator
ΔP_7	Pressure Drop across Orifice Plate
T_1	Inlet Air Temperature
T_2	Heated Air Temperature
T_3	Turbine Inlet Temperature
T_4	Turbine Outlet Temperature
T_5	Separator Outlet Temperature
T_6	Mixture Dry Bulb Temperature
T_7	Superheated Steam Temperature
T_{amb}	Ambient Air Temperature
T_{fw}	Boiler Feedwater Temperature
T_{oil}	Oil Temperature
WBD	Mixture Wet Bulb Depression
m_{sep}	Mass of Separated Liquid Sample
Δt	Time Elapsed During Sample Collection

In summary, the above steps which are listed and discussed were implemented to insure that data was collected at steady state operation and that safety threats to the system and operator were avoided.

Chapter VI

Axial Flow Centrifugal Separator Design

This research aims to develop an improved system for recovering moisture from a pressurized PEM fuel cell exhaust stream using a turbocharger and moisture separator. The moisture separator that was developed removed the liquid condensate from the humid air stream after the stream had expanded through the turbine side of the turbocharger. The axial flow centrifugal separator design section gives a detailed description of the design of the moisture separator used in this investigation.

The primary design requirement was the removal of liquid condensate that forms in the humid stream as a result of lowered temperature and pressure caused by expansion. The liquid condensate is in the form of small particles or droplets that are entrained in the flow. Separation is achieved by imposing an axi-symmetric swirl on the flow. The swirl or rotation imparts a centrifugal acceleration on the droplets in the flow and causes the higher density droplets to move to the outside of the flow. Strong swirl was accomplished by employing an axial flow swirl element with spiral grooves cut into the surface.

The second design requirement was the avoidance of a large pressure drop across the separator. This was achieved by employing a swirl element with a streamlined contour that minimized flow separation. The profile of the swirl element was adapted from a standard NACA airfoil design. Also, the cross-sectional area of the spiral grooves

at the widest diameter of the swirl element was set equal with the inlet area of the separator housing that directs the flow over the swirl element. The conservation of area serves to reduce an adverse pressure gradient in the flow that might break up the droplets.

This chapter is organized into sections describing the various aspects of separator design as follows:

1. Separator Geometry
    - Swirl Element Profile
    - Settling Length Calculation
    - Droplet Radius Determination
    - Swirl Angle Calculation
    - Vane Height Calculation
2. Separator Housing and Construction

V.1 Separator Geometry

The centrifugal separator is a well documented device for the removal of small droplets or particles from a gas or liquid stream. It operates on the principle that it causes the incoming flow to rotate strongly resulting in the migration of more dense particles to the outside of the flow. There are two basic types of centrifugal separators differentiated by how the flow enters the separator. The first type is a tangential flow separator. The flow enters tangentially into a pipe section and follows a downward spiral path through

the separator before reversing direction and exiting axially through the top of the separator. The tangential flow through the separator generates a strong swirl in the flow, but results in a large pressure drop across the separator. The conventional separator available for use in the experimental apparatus is a tangential flow separator.

The other type of centrifugal separator is an axial centrifugal separator. In this design, the flow enters the separator axially and begins to swirl after passing over a swirl generating element. The swirl element generally consists of a streamlined body with spiral vanes attached that impart a tangential velocity to the otherwise axial flow. The entrained particles are subsequently moved to the outside of the flow where they are removed downstream of the swirl element.

This investigation will seek to utilize the latter design, the axial flow centrifugal separator, to recover liquid water from the humid exhaust stream as a means of supplementing the requirements of a PEM fuel cell system.

VI.1.1 Swirl Element Profile

One of the major goals in the research is to avoid large pressure drops through the separator. Since the flow through the separator will travel axially over the swirl element, a streamlined profile is desired. To create the streamlined profile, a standard 2412 NACA airfoil design was chosen as the template (Ladson *et al.*, 1996). This airfoil design is well documented and is often found on light aircraft. Figure 6.1 shows a

standard NACA airfoil design and terminology.

Once the airfoil was chosen, the upper and lower surfaces were generated in AutoCAD and the upper and lower surfaces were separated. The upper surface was then revolved around the mean chord line to create the separator body. The body was then scaled while maintaining the original aspect ratio to fit the standard 3 inch clear PVC pipe that would be used as the housing of the separator.

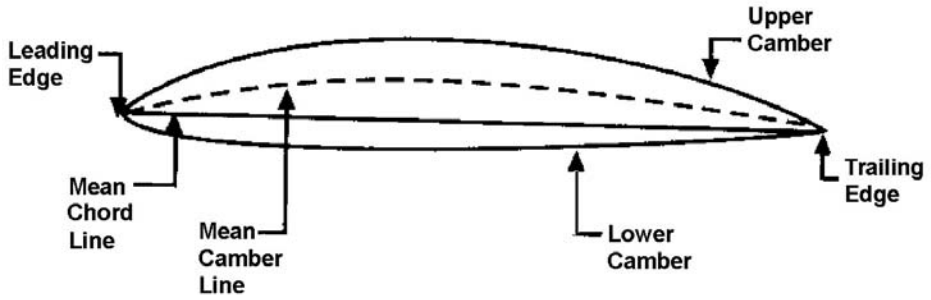

Figure 6.1 Standard Airfoil Design

V.1.2 Settling Length Calculation

This separator is being developed under the premise that its primary use would be in automotive fuel cell applications. In such an application, size is a major design consideration. The primary limiting factor for size of the separator body is settling length. Nieuwstadt and Dirkzwager (1995) provide an expression for the efficiency of an axial centrifugal separator of this design. This expression is shown in Equation 6.1. In

Equation 6.1, D is the diameter of the pipe through which the flow travels. In this investigation it is the diameter of the separator housing that contains the swirl element.

$$\frac{L_s}{D} = \frac{18\pi^2}{\alpha^2}\frac{1}{Re}\frac{\rho_f}{\rho_P - \rho_f}\left(\frac{W_{ann}}{r_d}\right)^2 \tag{6.1}$$

where

L_s = settling length

D = pipe diameter

$\alpha = 4\pi$

$Re = \frac{uD}{\nu}$, u = velocity of humid air stream, ν = kinematic viscosity

ρ_f = density of air stream

ρ_P = density of droplet

W_{ann} = width of annulus

r_d = droplet radius

Nominally sized 3 inch schedule 40 clear PVC was chosen for the housing due to its low cost, availability, and ease of use. This also limited the size of the swirl element to the interior diameter of the pipe. The width of the annulus (W_{ann}) is the height of the channel that turns the flow and imparts the swirl. The calculation for the channel height is presented in a later section. The radius of the droplet however was a measurement that was not readily known. This measurement had to be determined directly.

VI.1.3 Droplet Radius Determination

The experimental apparatus was slightly modified to facilitate the measurement of the radius of the droplets entering the separator. The exit of the turbine was normally fitted with a 1 ¼ inch pipe nipple that leads to a 1 ¼ inch tee. For the droplet measurement, the 1 ¼ inch tee was replaced with a 1 ¼ inch cross. Two sides of the cross served as inlet and exit passages and a third was fitted with a thermocouple as was the tee which was normally used. The remaining side of the cross was fitted with a 1 ¼ inch 90 degree elbow which led to a 1 inch nominal ball valve. The ball valve was fitted with a 1 inch pipe nipple. While the experimental apparatus was in operation, the cross allowed the exhaust from the turbine to split into two streams. One stream continued through the system while the other stream flowed into the branch installed on the cross. The ball valve allowed a sample of the humid stream to be vented into ambient air in order to obtain a sample.

During steady state operation, the valve was opened momentarily to allow the humid stream to flow into the atmosphere. For the droplet radius measurement, chilled, wax coated slides were used to obtain the samples. The wax coating prevented the slide from having a wetting surface where the droplet would spread out. The slides were chilled after prior attempts to obtain a sample were unsuccessful due to evaporation of the water droplet.

Once the sample was obtained on the slide, the slide was transferred to a

microscope fitted with a digital camera. Digital still images of the droplets were taken. There was also an image taken under the same settings as the droplet images of a gage wire for comparison. A representative image of the droplets is shown in figure 6.2 and the gage wire image is shown in figure 6.3.

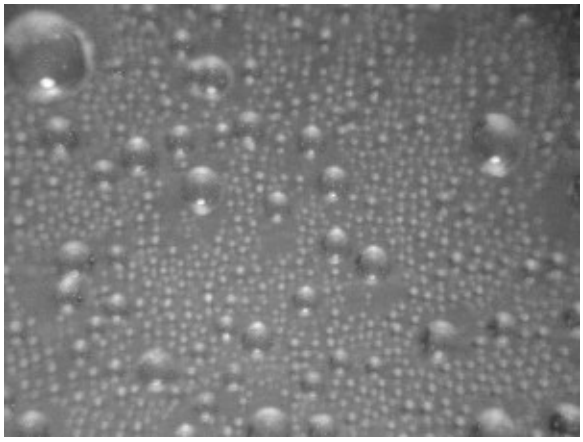

Figure 6.2 Humid Stream Droplet Image

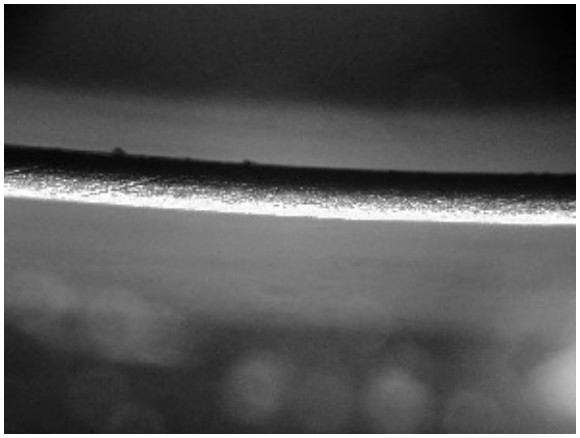

Figure 6.3 Gage Wire Used for Comparison

Once the images were acquired, they were displayed at the same resolution on the laboratory computer monitor and a ruled scale was used to compare the droplet sizes to

the gage wire as it appeared on the monitor. Several attempts were made to acquire an image of the gage wire and droplets on the same slide. These attempts were unsuccessful however due to differences in focal length for the wire and droplets. Since the wire was somewhat larger than the droplets, only the wire or the droplet could be focused on at any one time. The gage wire had a thickness of 0.0635 mm (0.0025 in.) and the droplets ranged in size from $1/10^{th}$ to $1/4^{th}$ of the size of the gage wire. The average droplet size was found to be approximately 0.01 mm (0.0005 in.).

Once the droplet radius was known, then the settling length for the separator could be determined. The settling length was calculated to be 3 cm (1.2 in.) for the separator to be used in this investigation. This length is actually less than the length of the swirl element itself and the minimum settling length that can be tested is 30 cm. The maximum settling length that can be tested is 61 cm.

VI.1.4 Vane Angle Calculation

A vane geometry that produces a tangential velocity component that is twice the axial velocity component at the trailing edge of the vanes is best for turning the flow without causing separation (Nieuwstadt and Dirkzwager, 1995). Equation 6.2 shows the relationship between the tangential and axial flow components.

$$u_t = 2u_a \tag{6.2}$$

The velocity of the humid stream exiting the turbine was calculated to be approximately 17.5 m/s. Based on Equation 6.2, the required tangential velocity is 35 m/s. The vane angle required to swirl the flow with that tangential velocity was calculated to be 63°. This calculation is shown in Appendix B.

VI.1.5 Vane Height Calculation

Once the swirl element profile and vane angle were determined, the only remaining parameter to specify was vane height. The swirl element was designed with a streamlined profile that increases in diameter to a maximum equal to the inside diameter of the separator housing. The element then decreases in diameter to a minimum at the point of contact with the chilled water pipe running through its center. In order to avoid an adverse pressure gradient throughout the separator section that could lead to droplet breakup and decreased separator efficiency, the total area of the spiral channels at the largest diameter location was set equal to the cross-sectional area of the inlet pipe.

There were some practical considerations that simplified the vane height calculation however. The spiral channels were cut with a standard ½ inch round tip mill bit on a four axis mill. The mill bit set the channel width at 1.27 mm (0.5 in.). The swirl element has a perimeter of 24 mm (9.4 in.) which accommodates an integer count of 18 channels. Material and manufacturing considerations limit that number to 15 though. Any number of channels greater than 15 results in a channel wall thickness of 1.5 mm (.06 in.). With any channel wall thickness less than or equal to 1.5 mm there is the

possibility of distortion in the metal during manufacturing and separator construction. The number of channels was set to 15 leaving channel depth as the only variable. Iterating until the total area of the channels equaled the cross-sectional area of the inlet pipe resulted in a vane height of 17.8 mm (0.7 in.). The iterations can be found in Appendix B. Figure 6.4 shows a cross section of the swirl element at the largest diameter.

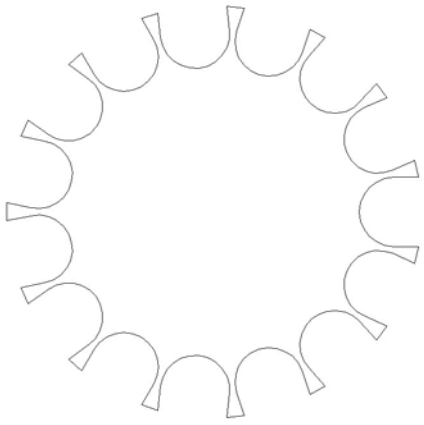

Figure 6.4 Cross Section of Swirl Element at Largest Diameter

VI.2 Separator Construction

Once the profile, vane angle, and vane height were known, the swirl element could be constructed. A 3-D model was generated in Catia® for visualization purposes and 2-D drawings were created in AutoCAD® to aid in the manufacturing of the aluminum swirl element. Figures 6.5a and 6.5b show the 3-D representation. Figure 6.6a shows the swirl element as it would be seen from a perspective located at the entrance to the separator. The element is oriented slightly at an angle in this view that shows the beginning of the spiral grooves. Figure 6.5b shows the spiral grooves of the swirl

element in more detail as they follow the contour of the main body. Both views show the leading edge of the swirl element that first encounters the humid stream.

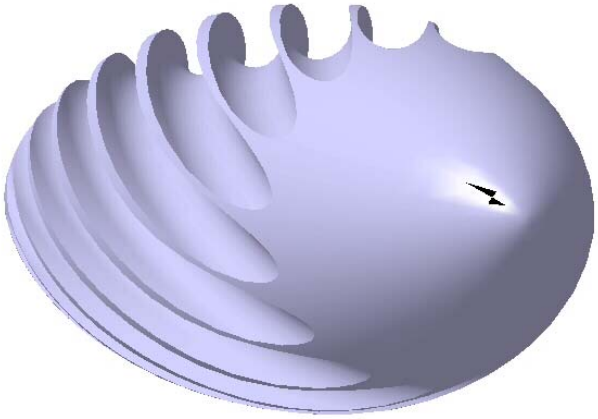

Figure 6.5a Axial Flow Swirl Element Model Created in Catia – View 1

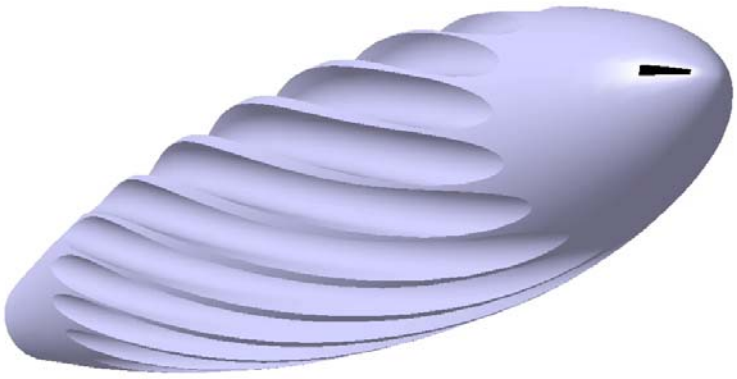

Figure 6.5b Axial Flow Swirl Element Model Created in Catia – View 2

The 2-D drawings that were generated in AutoCAD were used by a four axis CNC mill to machine the element. The element was then installed into the separator housing. The following text describes the separator housing and swirl element combination in more

detail. Figure 6.6 shows the separator in schematic form.

The humid stream enters the separator section from the turbine through a length of schedule 40 PVC pipe. The end of the pipe is fitted with a 1 ¼ inch to 2 inch bushing that leads into a 2 inch to 3 inch long turn wye. The separator has a vertical orientation and the humid stream flows downward in order to take advantage of gravitational effects on the separation process. The condensate will have a tendency to accumulate at the lowest point in the system, so any other orientation will result in a concentration of condensate on one side of the interior of separation housing. The long turn wye has one outlet to the upward direction and one outlet to the downward direction. The upward outlet is fitted with a 3 inch hex bushing that has had the hex rounded off flush with the outer diameter. The bushing is capped with a 3 inch end cap. The end cap is tapped and fitted with a 1 inch to ¾ inch threaded bushing. A ½ inch compression fitting is installed into the bushing. The compression fitting holds a ½ inch copper pipe in place that runs through the length of the separator and protrudes through the other side. The pipe allows for chilled water to be pumped through the separator for the purpose of cooling the swirl element but that feature was not utilized during this investigation. The downward facing exit of the long turn wye is leads to a 3 inch ID, 76 mm (30 inch) length of clear PVC.

The clear PVC serves as the housing for the axial flow swirl element which is located according to the desired settling length. The swirl element is made of a bar of 2017 alloy aluminum and has an outer diameter approximately equal to the interior diameter of the housing. There are fifteen spiral grooves cut into the surface. The spiral

grooves serve to impart an axi-symmetric swirl to the humid air stream causing the more dense liquid droplets to move to the outside of the flow and travel along the inside of the clear PVC housing. The liquid droplets are removed from the flow downstream of the swirl element. The ½ inch copper pipe runs through the center of the of the swirl element which is constrained in place by friction between the aluminum surface and the interior surface of the housing. As an added measure, two set screws are installed at the bottom of the swirl element to assist in holding it in place by securing it to the copper pipe.

The separator housing terminates in a 3 inch coupling. The other end of the coupling is fitted with a 3 inch to 2 inch flush bushing. The inside of the bushing is threaded with a length of 2 inch pipe that extends back into the housing. Once the liquid droplets have been separated out of the humid stream, the stream exits the separator housing through the 2 inch pipe. The bushing that the 2 inch pipe threads into is connected to a 3 inch 90 degree elbow. The exit of the elbow is fitted with a 3 inch to 2 inch reducing bushing with a 3 inch length of 2 inch pipe inserted into the bushing. This short piece of pipe is the outlet for the separator. 2 inch flexible reinforced piping is attached to the outlet with a pipe clamp and directs the stream outside into the atmosphere. The liquid condensate is removed from the separator through two ports installed on either side of the coupling attached to the end of the clear PVC housing. These ports are located at the intersection of the clear PVC and the bushing inside the coupling so each piece was tapped and fitted with compression fittings to allow a passage for the water to escape. Two 1/8 inch plastic hoses direct the separated condensate into a collection container.

Both the 3 inch long turn wye and the 3 inch 90 degree elbow have fittings installed to allow for the insertion of thermocouples into the flow to measure the temperature before and after the swirl element (T_4 and T_5, respectively). The clear PVC pipe is tapped and threaded with barb fittings. This allows for a differential pressure measurement to be taken across the swirl element with a U-tube manometer more specifically a Dywer Instruments 0 to 16 inH_2O Manometer. The ends of the manometer are attached to the pressure taps with clear rubber hose. Figure 4.8 shows the moisture separator in schematic form.

In summary, this section has provided a detailed description of the design of the moisture separator used in this investigation and the integration into the test apparatus.

Chapter VII

Data Processing and Results

The data processing and results chapter describes the methods and calculations used to evaluate the performance of the moisture separator in addition to the results obtained during the experimental trials. The primary indicators of separator performance are separation efficiency and pressure drop. The pressure drop across the separator was straightforward to determine as it consisted of a single direct measurement. The separator efficiency however was more complex to calculate and was defined as the ratio of the amount of liquid recovered from the separator to the amount of condensate that was available in the humid stream for removal. Experimental uncertainties for these measurements are also presented. All calculations were performed with Engineering Equation Solver (EES). A complete listing of the equations used to perform the calculations can be found in Appendix C.

VII.1 Air Flow Rate

The compressed air flow rate through the system was measured with a rotameter. The rotameter required a correction when the operating conditions of the working fluid were different from the standard conditions that the rotameter was graduated for. Equation 7.1 gives the correlation between the compressed air mass flow rate and rotameter reading.

$$\dot{m}_{\text{ma}} = RM_{\text{air}}\left(\frac{P_1 \cdot T_{\text{std}}}{T_1 \cdot P_{\text{std}}}\right) \tag{7.1}$$

The accuracy of the air flow rotameter was checked with a thermal flow meter. After the air exits the rotameter it enters the electric resister heating section. The amount of power dissipated in the heater section and imparted to the air was measured with a wattmeter. Equation 7.2 shows an energy balance for the heater section control volume. This Equation correlates the air mass flow rate to the power required to heat it.

$$\dot{m}_{\text{air,b}} = \frac{\dot{Q}_{\text{heater}}}{C_{\text{P}}\left(T_2 - T_1\right)} \tag{7.2}$$

The mass flow rate of air from the energy balance ($\dot{m}_{\text{air,b}}$) and mass flow rate of air obtained from the rotameter correlation were shown to be within 5% of each other.

The moisture contained in the air as it entered the system from the building supply had to be determined as well. To facilitate this measurement, a valve was used to throttle compressed air across a humidity probe at the inlet to the system. The temperature (T_1), pressure (P_{atm}), and relative humidity (ϕ_1) of the air at the location where the humidity probe was located allowed the humidity ratio function of EES to calculate the humidity ratio (w_1) of the incoming compressed air. The humidity ratio is defined in Equation 7.3. The mass flow rate of water vapor entering the system with the compressed air is determined from the humidity ratio of the incoming air and the conservation of mass

statement for the compressed air stream shown in Equation 7.4.

$$\omega_1 = \frac{\dot{m}_{wv}}{\dot{m}_{da}} \tag{7.3}$$

$$\dot{m}_{\mathrm{ma}} = \dot{m}_{\mathrm{da}} + \dot{m}_{wv} \tag{7.4}$$

The expression for the mass flow rate of water vapor entering the system with the building compressed air stream is obtained by combining Equations 7.3 and 7.4. This expression is shown in Equation (7.5).

$$\dot{m}_{wv} = \frac{\dot{m}_{ma}}{\left(\frac{1}{w_1} + 1\right)} \tag{7.5}$$

The mass flow rate of dry air $(\dot{m}_{da})$ was then readily calculated from Equation 7.4 once the mass flow of vapor and compressed air were obtained.

VII.2 Steam Mass Flow Rate

The steam injection system added a constant mass flow of superheated steam to the compressed air stream. The steam flow rate into the system was determined by measuring the pressure drop across an orifice plate after the steam left the boiler, and then correlating the pressure drop to a volumetric flow rate. The correlation Equation used is

shown in Equation 7.6.

$$\dot{V}_{\text{steam}} = C \cdot Y \cdot F_{\text{A}} \cdot A_{\text{o}} \left(\frac{2\Delta P_7}{\rho_7 (1-\beta^4)} \right)^{1/2} \tag{7.6}$$

β is the ratio of the orifice diameter d to the inside pipe diameter D and A_{o} is the area of the orifice opening. ΔP_7 is the pressure drop measured across the orifice plate. C, Y, and F_{A} are coefficients determined from empirical correlations (Bean, 1971). These correlations are shown below.

$$\text{C} = K_{\text{SB}}(1 - \beta^4)^{1/2} \tag{7.7}$$

Equation 7.7 shows the discharge coefficient for the orifice flow meter. Equations 7.8a through 7.8c show the correlations for the constant K_{SB}.

$$K_{\text{SB}} = \left[0.5991 + \frac{0.0044}{D} + \left(0.3155 + \frac{0.0175}{D} \right) \left(\beta^4 + 2\beta^{16} \right) \right] +$$

$$\left[\frac{0.00052}{D} - 0.000192 + \left(0.01648 - \frac{0.00116}{D} \right) \left(\beta^4 + 4\beta^{16} \right) \right] \lambda \tag{7.8a}$$

$$\lambda = \frac{1000}{\sqrt{\text{Re}_D}} \tag{7.8b}$$

$$\mathrm{Re}_D = \frac{V \cdot D}{\nu} \tag{7.8c}$$

All properties were calculated based on conditions upstream of the orifice flow plate. Re_D is the Reynolds number for the steam flow in the pipe upstream of the orifice flow plate. V is the velocity and ν is the kinematic viscosity of the steam flow.

The expansion coefficient (Y) corrects for the differences in fluid density at the upstream property measurement location and the orifice. Equation 7.9 gives the correlation for the expansion coefficient.

$$Y = 1 - \left(0.41 + 0.35\beta^4\right)\left(\frac{\Delta P_7}{27.73 \cdot k \cdot P_{7,abs}}\right) \tag{7.9}$$

The symbol k represents the specific heat ratio of the steam based on the upstream conditions. This parameter was calculated using the specific heat function of EES. A value of 1.37 was used.

The thermal expansion factor (F_A) corrects for the dimensional changes of the pipe and orifice due to thermal expansion. Equation 7.10 gives the correlation for the thermal expansion factor (ASME, 1990).

$$F_A = 1 + \left(\frac{2}{1-\beta^4}\right)\left(\alpha_{OP} - \beta^4 \alpha_P\right)\left(T_7 - T_{meas}\right) \tag{7.10}$$

The thermal expansion coefficients of the pipe and orifice plate are α_P and α_{OP}, respectively. T_{meas} is the temperature at which the pipe and orifice dimensions were measured, or in this case ambient room temperature.

The discharge coefficient depends on Reynolds number which in turn depends on the velocity of the steam flow. The velocity however is the parameter that is being sought in the volumetric flow rate calculation that is shown in Equation 7.6. A solution is obtained by using an iterative technique that is implemented in the EES program. A guess value is used to start the routine which runs until the error between two consecutive iterations is less than 0.001 m/s. Once convergence is obtained, the steam volumetric flow rate allows for the calculation of steam mass flow rate from Equation 7.11.

$$\dot{m}_{st} = \rho_7 \cdot \dot{V}_{steam} \tag{7.11}$$

An energy balance performed on the boiler serves as a check for the steam mass flow rate obtained in Equation 7.11. The energy balance is shown in Equations 7.12 and 7.13.

$$\dot{m}_{steam,b} = \frac{\dot{Q}_{boiler}}{h_7 - h_{fw}} \tag{7.12}$$

$$\dot{Q}_{boiler} = \sqrt{3} \cdot V_{3\phi} \cdot i_{3\phi} \tag{7.13}$$

In Equation 7.12, the enthalpies of the steam and feedwater, (h_7) and (h_{fw})

respectively are calculated based on the properties measured at the inlet and outlet of the boiler. In Equation 7.13, $V_{3\phi}$ and $i_{3\phi}$ are the three phase line voltage and current supplied to the boiler.

VII.3 Mixed Stream Properties

The dry air stream is injected with the superheated steam and mixed at location 3. The mixed stream then expands through the turbine before entering the moisture separator. In order to determine the amount of condensate available for removal it is necessary to know the humidity ratio of the humid stream before and after the turbine. The humidity ratio of the humid stream before entering the turbine was calculated using Equation 7.14.

$$w_3 = \frac{\dot{m}_{\text{vap}} + \dot{m}_{\text{st}}}{\dot{m}_{\text{da}}} \tag{7.14}$$

An Equation similar to 7.14 cannot be used for w_4 because the expansion through the turbine results in a drop in temperature and pressure which causes some of the vapor in the stream to condense into liquid. The humidity ratio of the turbine outlet (w_4) is dependant on the temperature, pressure and relative humidity at that location and the relative humidity is dependant upon the phase.

The EES program employed a routine for the determination of the phases present in the exhaust stream. First, the relative humidity at the turbine exit was calculated using the properties at the exit (T_4 and P_4) and the humidity ratio of the mixed stream at the turbine inlet (w_3). If the resulting relative humidity was greater than 100%, then the exhaust stream had two phases present at the temperature and pressure conditions of the outlet. The relative humidity used to calculate the humidity ratio (w_4) in this case was 100% since the humid stream is saturated at T_4 and P_4.

If the resulting relative humidity calculated from T_4, P_4, and w_3 was less than 100%, then the exhaust stream contained only a single gas phase. The mass flow of condensate in that case is 0 g/s.

In the case where two phases are present in the turbine exhaust stream, a mass balance of the turbine control gives the mass flow of the liquid condensate ($\dot{m}_{cond}$) available for recovery from the separator. Equation 7.15 shows the mass balance for the turbine control volume.

$$\dot{m}_{cond} = \dot{m}_{da}\left(w_3 - w_4\right) \tag{7.15}$$

At this point, the separator efficiency can be calculated based on the ratio of the mass flow rate of liquid that was recovered from the separator during the experimental trials ($\dot{m}_{sep}$) to the mass flow rate of liquid condensate in the turbine exhaust ($\dot{m}_{cond}$). This calculation is shown in Equation 7.16.

$$\eta_{sep} = \frac{\dot{m}_{sep}}{\dot{m}_{cond}} \tag{7.16}$$

In summary, the evaluation of separator performance was straightforward in the case of pressure drop but required a series of calculations for the separator efficiency. The next section presents the experimental results for the separator.

VII.4 Experimental Results

The experimental trials that were conducted to evaluate the performance of the moisture separator were carried out for three different settling lengths. The settling length is defined as the length from the largest radius of the swirl element to the location where droplets are actually removed from the flow. The settling length was adjusted by changing the axial location of the swirl element in the separator housing.

In addition to three different settling lengths, the experimental trials were conducted for a range of heated air conditions. Altering the heated air temperature allowed some variation in the turbine inlet conditions which in turn affected the amount of condensate available in the stream for recovery. The turbine inlet conditions are restricted based upon the exhaust conditions of a PEM fuel cell. The operating temperature range was shown in Chapter II to be between 70 °C and 80 ° C.

In total, twenty five experimental trials were conducted to evaluate separator performance. Table 7.1 shows the test matrix used for the experiments. The twenty five

cases represent three settling lengths over a range of heated air temperatures. The Error Propagation Tool of EES was used to calculate experimental errors for the experimental trials. The results from that analysis can be found in Table 7.2. The standard uncertainty of the separation efficiency was shown to be approximately 9 % for the first experimental trial. The variable that contributed most to the uncertainty of the separator efficiency is the compressed air inlet pressure (P_1). One way to reduce the influence of the error by P_1 would be a new calibration. Another way would be to replace the pressure gauge with a new gauge altogether.

Table 7.1 Parameter Matrix for Experimental Conditions

Variable Parameters		
Experiment	Swirl Element Position	Heater Setting
		ºC
1	1	70
2	1	65
3	1	60
4	1	55
5	1	50
6	1	45
7	1	40
8	1	35
9	1	30
10	1	25
11	2	75
12	2	70
13	2	65
14	2	60
15	2	55
16	2	50
17	2	45
18	2	40
19	2	35
20	2	30
21	3	70
22	3	60
23	3	45
24	3	35
25	3	20

Position	Settling Length	
1	61 cm	Maximum
2	12 cm	Minimum
3	46 cm	Middle

VII.4.1 Separator Efficiency and Comparison

It was shown in Chapter II that the operating temperature of the exhaust of a PEM fuel cell fell within a range of 70 ºC and 80 ºC and that the humidity ratio required was approximately 0.115. The experimental test conditions resulted in a mixture temperature range at the turbine inlet between 82.5 ºC and 77.5 ºC for all three positions of the swirl element. The humidity ratio averaged from 0.125 for the minimum settling length trials to 0.118 for the maximum settling length trials. The experimental conditions closely matched the conditions prescribed for PEM fuel cells.

Table 7.2 Summary of Uncertainty Analysis for Separation Efficiency

Measurement	U_{xi} [a]	Influence Coefficient, $\frac{\partial \eta_{sep}}{\partial x_i}$	$U_i^2 = \left(U_{xi} \frac{\partial \eta_{sep}}{\partial x_i} \right)^2$	% of Uncertainty	Basis	Source
m_{sep}	1 g	0.0043	0.00002	0.24	resolution	(1)
Δt	0.1 s	-0.079	0.00006	0.01	resolution	(1)
P_{atm}	1.3 mmHg	-0.017	0.00049	0.26	resolution	(1)
P_1	0.5 psi	0.12	0.0036	49.35	calibration	(2)
P_4	0.5 inH_2O	-0.04	0.0004	4.78	resolution	(1)
P_7	0.25 psi	-0.1	0.00063	8.59	calibration	(2)
ΔP_7	0.09 inH_2O	-0.3	0.00073	9.43	calibration	(3)
ϕ_1	0.003	-2.18	0.00004	0.55	calibration	(4)
RM_1	0.1	0.2	0.0004	3.77	resolution	(1)
T_1	0.22 ºC	-0.04	0.00008	1.17	calibration	(3)
T_4	0.05 ºC	0.79	0.002	19.91	calibration	(3)
T_7	0.44 ºC	0.02	0.00008	0.97	calibration	(3)
		sum of U_i^2 =	0.0085			
		Expanded Uncertainty B =	0.09			

Sources: (1) Physical Inspection (2) Calibrated by Omega (3) Calibration (4) Calibrated by Vailsala

The performance of the moisture separator is based upon the amount of moisture recovered from the humid stream and the pressure drop across the separator. Equation 7.16 shows the equation used to determine the separator efficiency. Figure 7.1 shows a plot of liquid recovered from the stream versus the amount of condensate available for recovery. This plot is for the maximum settling length of 61 cm (24 in).

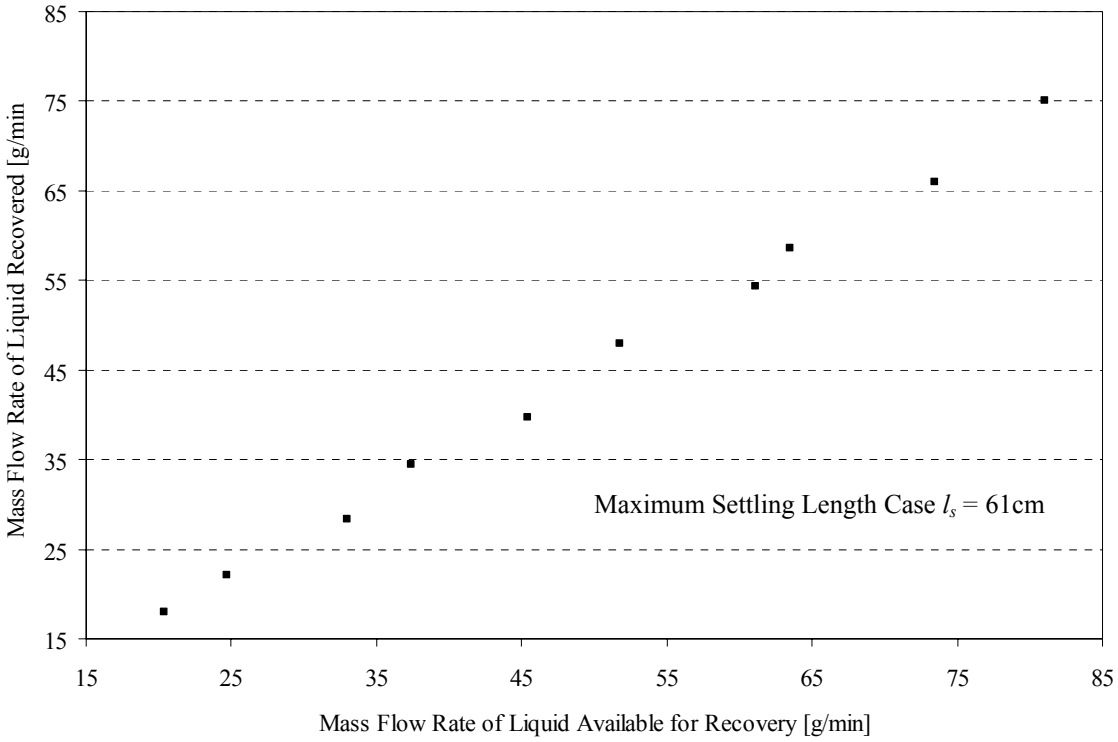

Figure 7.1 Recovered Liquid versus Available Condensate for 61cm Settling Length

The plot shows that as the available condensate increases, the mass flow rate that is recovered increases as well. A Microsoft Visual Basic Program was used to plot the separation efficiency versus the turbine inlet temperature (Jeter 2004). The plots for the maximum settling length and the minimum settling length can be found in Figures 7.2 and 7.4 respectively. The middle separating case however had too few data to provide

meaningful results. The efficiencies ranged from 86 to 93% for the maximum settling length case. In comparison, the conventional moisture separator was found to have an efficiency of 65%. A curve was fitted through the data with the program but the observed alpha risk is higher than 5% meaning that the regression line is not statistically different from a line representing the average of the data. In fact, a line representing the average of the sample falls within the error limits of the regression line.

Figure 7.3 shows a plot of liquid recovered from the stream versus the amount of condensate available for recovery. This plot is for the minimum settling length of 30 cm (12 in). This plot exhibits the same trend that was observed in the maximum settling length case of 61 cm. The amount of moisture that is recovered from the stream increases directly with the amount of liquid condensate that is available for separation.

The plots of mass flow rate of liquid separated versus mass flow rate of liquid available in Figure 7.5 for the middle settling length of 46 cm exhibits the same behavior as the other two cases. The amount of liquid recovered increases directly as the amount of liquid available for separation increases.

Table 7.3 presents efficiency and pressure drop results for the improved and conventional separators. The mass flow rate of moisture recovered and the mass flow rate of liquid available for recovery are shown along with the separator efficiency. The uncertainty for the efficiency calculation is provided along with each uncertainty as well. The uncertainty calculation was determined as prescribed in the text above.

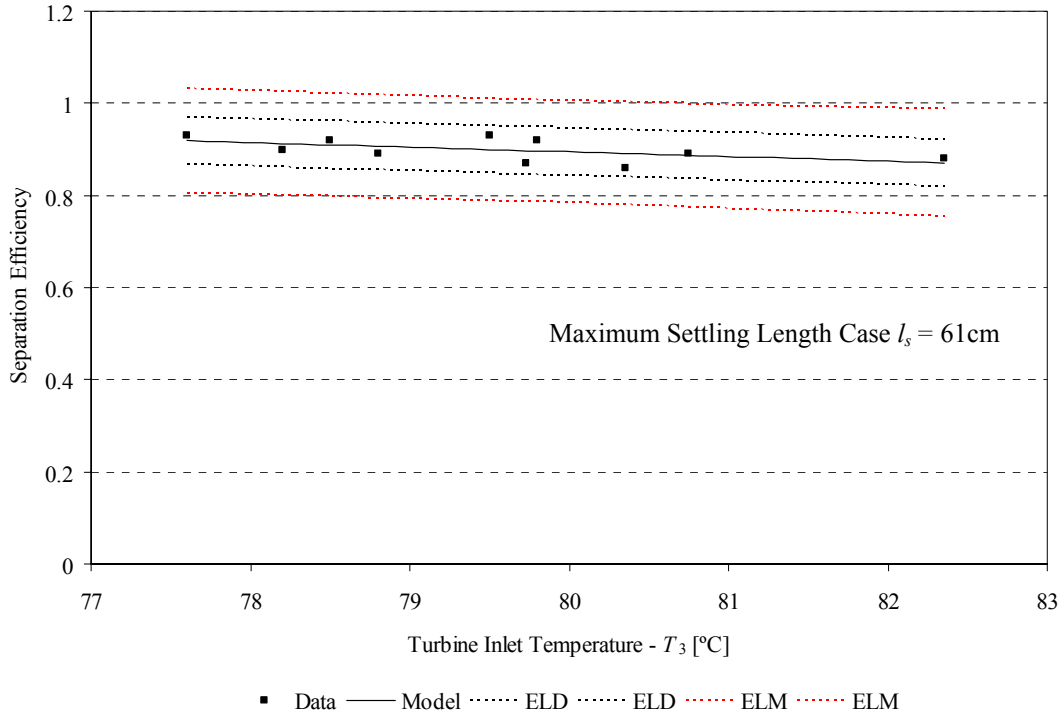

Figure 7.2 Separator Efficiency versus Turbine Inlet Temperature for 61 cm Settling Length

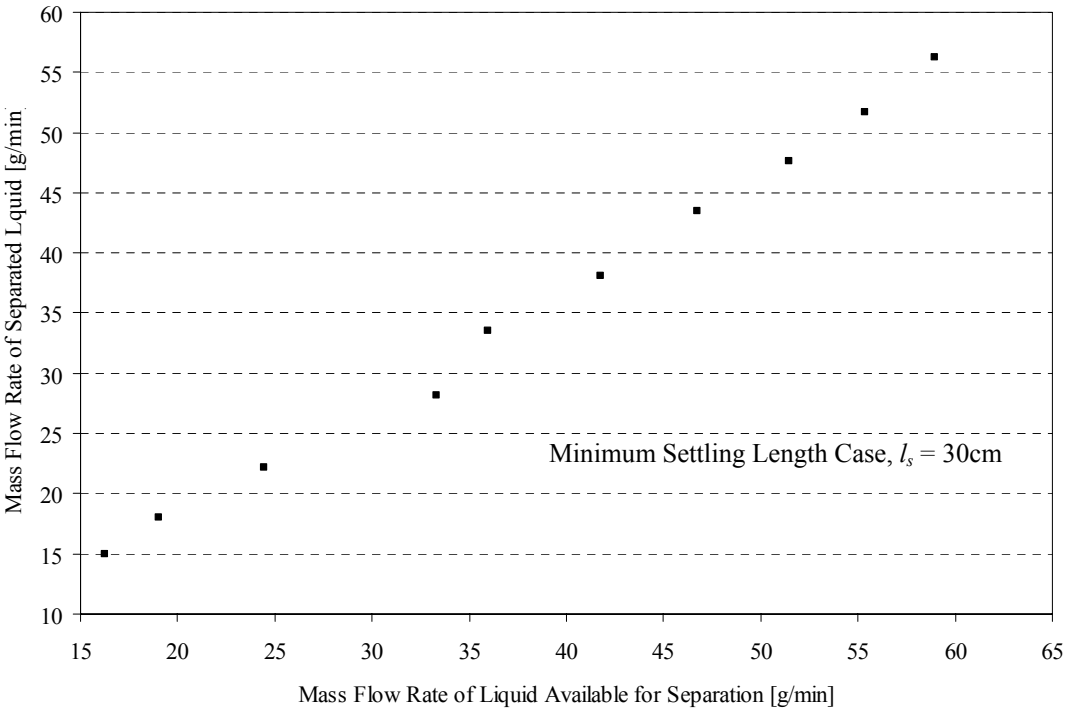

Figure 7.3 Recovered Liquid versus Available Condensate for 30 cm Settling Length

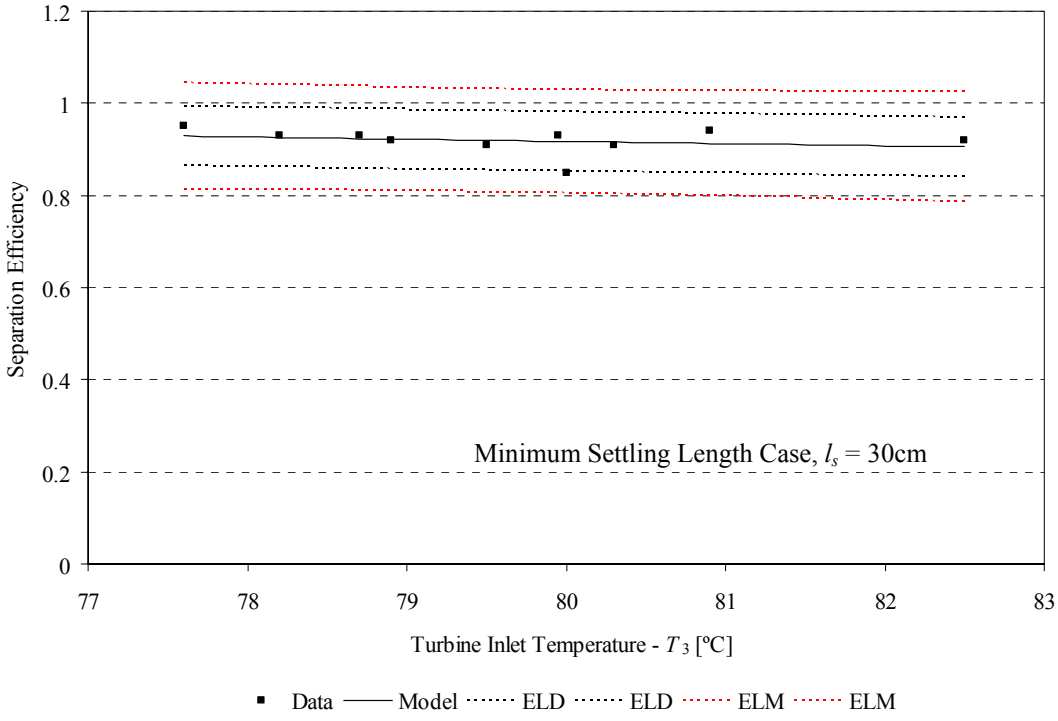

Figure 7.4 Separator Efficiency versus Turbine Inlet Temperature for 30 cm Settling Length

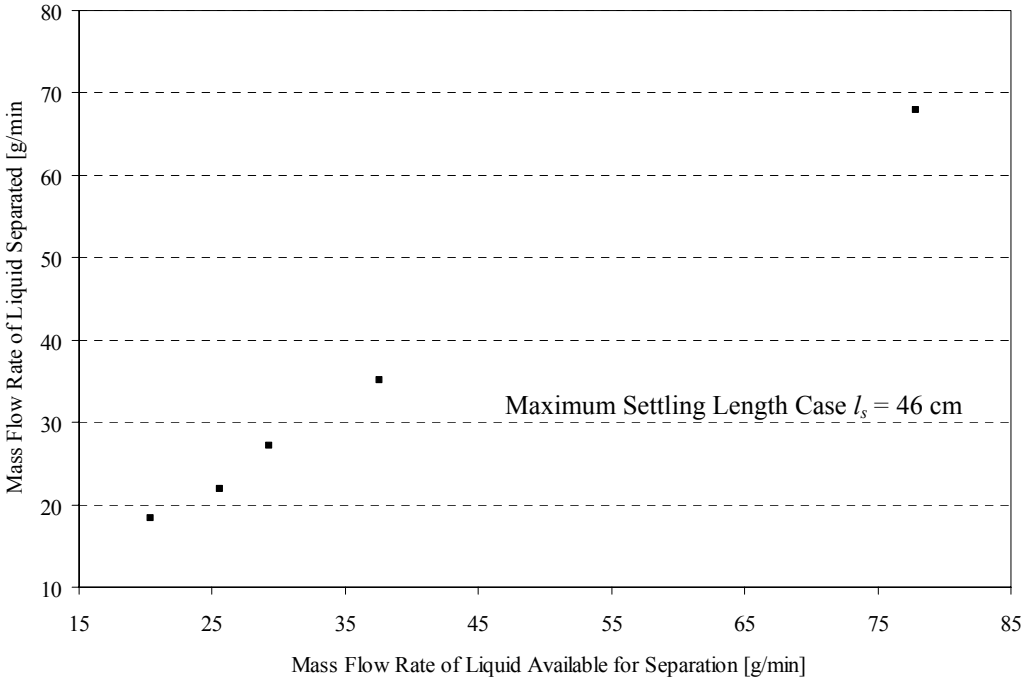

Figure 7.5 Recovered Liquid versus Available Condensate for 46 cm Settling Length

T**able 7.3** Experimental Results for Improved and Conventional Separators

Trial	$\dot{m}_{sep}$	$\dot{m}_{cond}$	η_{sep}	U	ΔP
	g/min	g/min	%	%	in. H_2O
1	18.03	20.41	0.88	0.09	7.0
2	22.03	24.67	0.89	0.07	6.7
3	28.40	32.97	0.86	0.05	6.7
4	34.44	37.35	0.92	0.05	6.7
5	39.65	45.41	0.87	0.04	6.7
6	48.00	51.79	0.93	0.03	6.7
7	54.31	61.07	0.89	0.03	6.6
8	58.52	63.46	0.92	0.03	6.6
9	66.00	73.42	0.90	0.02	6.6
10	75.00	81.00	0.93	0.02	6.6
11	15.00	16.29	0.92	0.13	7.1
12	18.00	19.06	0.94	0.11	7.1
13	22.20	24.43	0.91	0.08	7.1
14	28.20	33.30	0.85	0.05	7.1
15	33.50	35.97	0.93	0.05	7.1
16	38.10	41.79	0.91	0.04	7.1
17	43.50	46.76	0.93	0.04	7.0
18	47.60	51.49	0.92	0.04	7.0
19	51.73	55.37	0.93	0.03	6.9
20	56.20	58.98	0.95	0.03	7.0
21	18.40	20.41	0.90	0.09	7.0
22	21.90	25.54	0.86	0.07	7.0
23	27.19	29.31	0.93	0.06	7.0
24	35.18	37.52	0.94	0.05	6.9
25	67.90	77.85	0.87	0.02	6.9
Conventional	11.97	18.41	0.65	0.11	21.3
Separator	20.80	32.50	0.64	0.05	20.8

The pressure drop across the improved centrifugal separator was also measured with the swirl element absent. This measurement provided the pressure drop of the separator housing only and was found to be 1 in H_2O. The pressure drop across the separator that is listed in Table 7.3 was measured during the experimental trials with the

swirl element in place. The pressure drop across the improved separator design was found to be 35% of the pressure drop across the conventional separator.

In summary, this chapter presented the calculations necessary for evaluation of separator performance. Equations 7.1 through 7.15 were used for determination of liquid water available for recovery by the separator. Equation 7.16 was used to calculate the separation efficiency. The improved separator design was shown to have a moisture separation efficiency of 90% while the conventional separator only had 65% efficiency. The pressure drop across the improved design was found to be only 35% of that across the conventional separator. Experimental data collected during experimental trials are in Appendix D.

Chapter VIII

Discussion and Recommendations

This chapter aims to provide a discussion of the major findings of this investigation and to provide recommendations for future phases of this project. The goal of this research is to document an improved moisture recovery device for a PEM fuel cell system. This chapter will evaluate the design for compatibility with the proposed PEM fuel cell system. In addition, the performance of the separator system is compared to that of a conventional separator for the recommended operating conditions.

VIII.1 Discussion

The fuel cell system that was proposed and discussed earlier is a PEM fuel cell that produces a hot and humid pressurized exhaust stream. The stream exits the fuel cell between 70 and 80 °C (176 °F) and 3.1 bar (30 psig). The dry air mass flow rate and water vapor mass flow rate requirements were shown to be 1930 g/min 223 g/min, respectively. These conditions resulted in a humidity ratio of 0.1157. All experimental trials conducted during this investigation maintained a turbine inlet temperature between 77 and 83 °C. The humidity ratios ranged between 0.1150 and 0.1240. The experimental trials were conducted under operating conditions very near those of a PEM fuel cell.

It was shown in Chapter II that the water requirement for the reformer is 181

g/min and that 81% of the moisture content of the pressurized stream would have to be recovered to supply the requirements of the fuel cell system. The steam injection system was delivering approximately 360 g/min of steam to the compressed air stream during steady state operation. Table 7.3 shows that a only 81 g/min of condensate were available for recovery during the cases where the swirl element was positioned to provide a maximum settling length. This was the highest amount available during any of the trials but is much lower than the 181 g/min required. The highest separation efficiency obtained during any of the trials was 95% with the lowest being 85%. These separation efficiencies are higher than the minimum 81% required to supply the fuel cell, even when taking into account the highest experimental uncertainty observed of 11%. The majority of the experimental trials that were conducted had experimental uncertainty for separation efficiency below 7%. In comparison, the available conventional separator was found to only have a separation efficiency of 65%. The uncertainty for the separation efficiency of the conventional separator is shown in Table 7.2. The improved centrifugal separator had a pressure drop that was found to be 65% lower than that of the conventional separator. These data are presented in Table 7.2.

VIII.2 Recommendations

This research has shown that an improved centrifugal separator can be used to successfully recover moisture from a pressurized humid stream. The improved separator design was able to achieve higher separation efficiency than that of the conventional separator while creating a lower pressure drop. Since the amount of water available for

separation was only 44% of the minimum amount required by the fuel cell system, this system was unable to recover enough liquid to supply the fuel cell system and needs improvement.

In order to condense enough water from the humid stream to meet the fuel cell requirements, the temperature of the stream at the inlet to the separator needs to be lowered further. With the current system, the steam exits the turbine at approximately 55 ºC. Calculations show that the stream needs to exit at 42.6 ºC to condense the 181 g/min that is required. One way of dropping the temperature of the stream is to install a heat exchanger between the turbine exit and the separator inlet. Placing the heat exchanger in this location would not diminish the energy extraction ability of the turbine.

Another way of lowering the temperature of the flow before it enters the separator is to utilize multiple turbines in the experimental setup. This setup would have an added advantage as well. Using two turbines would allow for the entire pressure drop available to be utilized to power the compressors.

More water may be able to be obtained by modifying the separator itself to include a heat exchanger. The swirl element was designed to allow for a co-axial channel to run through the center that could be used to flow chilled water through it. The chilled water would cause the swirl element to operate at a cooler temperature which would cause more liquid water to condense from the humid stream. In addition, the separator housing itself could be modified to include a heat exchanger. The housing used in this

investigation was constructed from clear PVC pipe for visualization purposes. However, it could be replaced with another material with a higher thermal conductivity to facilitate increased heat transfer across the pipe wall. The result would be increased droplet formation on the lower temperature wall.

It was also observed that there was no increase in separation efficiency at longer settling lengths. In fact, the minimum settling length of 3 cm that was calculated was less than the overall length of the swirl generator. In is inferred from this result that the separator could be made much more compact and still provide adequate separation.

In summary, this investigation has shown that an improved axial flow centrifugal separator can be used to successfully recover moisture from a pressurized humid stream, but no detailed computational fluid dynamics modeling or further experimental work was carried out to optimize the separator design that was investigated.

Appendix A

Calibrations and Uncertainty Data

A.1 Thermocouple Calibration and Uncertainty Data

Thermocouple Calibration Data						
Thermocouple	**1**	**2**	**3**	**4**	**5**	**6**
Location	1	2	3	4	5	6
Intercept	-0.215	-0.333	-0.228	4.020	0.014	-0.083
Slope	0.996	0.994	0.998	0.921	0.996	0.983
U	0.22	0.40	0.08	0.05	0.15	0.10
Thermocouple	**7**	**8**	**9**	**10**	**11**	**12**
Location	7	8	9	10	11	12
Intercept	-0.136	-0.074	-0.166	-0.426	-0.093	-0.152
Slope	0.988	1.004	1.004	1.002	1.000	1.001
U	0.44	0.08	0.22	0.28	0.05	0.18

The above table displays gain and offset data for the thermocouples used in this investigation. Uncertainty due to possible bias as determined from Standard Error of Estimate from linear regressions is presented as well.

A.2 Boiler Rotameter Calibration Data

file: Boiler_rotameter_Cal 9-Jan-04

Summary:

V_dot = 3.97*(Indicated Position) - 35.4

Parameters:

1 lbm = 0.453592 kg

density = 0.998403 kg/L

	time	time	time	start mass	end mass	mass in	Rotameter ind	m_dot actual	m_dot model	V_dot actual	V_dot actual	V_dot model
	min	sec	frac mins	(lbm)	(lbm)	(lbm)	(mm)	kg/min	kg/min	L/min	mL/min	mL/min
1	3	10.37	3.173	0.420	0.496	0.076	10	0.011	0.004	0.011	10.882	4.317
2	3	7.90	3.132	0.550	0.868	0.318	20	0.046	0.044	0.046	46.133	44.042
3	3	4.56	3.076	0.962	1.558	0.596	30	0.088	0.084	0.088	88.028	83.767
4	3	3.30	3.055	0.460	1.282	0.822	40	0.122	0.123	0.122	122.242	123.493
5	3	5.30	3.088	0.276	1.376	1.100	50	0.162	0.163	0.162	161.819	163.218
6	3	4.59	3.077	0.676	1.994	1.318	60	0.194	0.203	0.195	194.634	202.943
7	3	19.18	3.320	2.456	4.222	1.766	70	0.241	0.242	0.242	241.689	242.669
8	3	8.22	3.137	0.794	2.724	1.930	80	0.279	0.282	0.280	279.514	282.394
9	3	8.90	3.148	3.014	5.226	2.212	90	0.319	0.322	0.319	319.201	322.119
10	3	13.13	3.219	0.796	3.312	2.516	100	0.355	0.361	0.355	355.118	361.845
11	3	13.30	3.222	3.662	6.494	2.832	110	0.399	0.401	0.399	399.367	401.570
12	3	7.18	3.120	0.762	3.804	3.042	120	0.442	0.441	0.443	443.007	441.295
13	3	7.69	3.128	4.278	7.632	3.354	130	0.486	0.480	0.487	487.117	481.021
14	3	3.85	3.064	0.790	4.322	3.532	140	0.523	0.520	0.524	523.683	520.746
15	3	6.25	3.104	5.092	8.942	3.850	150	0.563	0.560	0.563	563.476	560.471

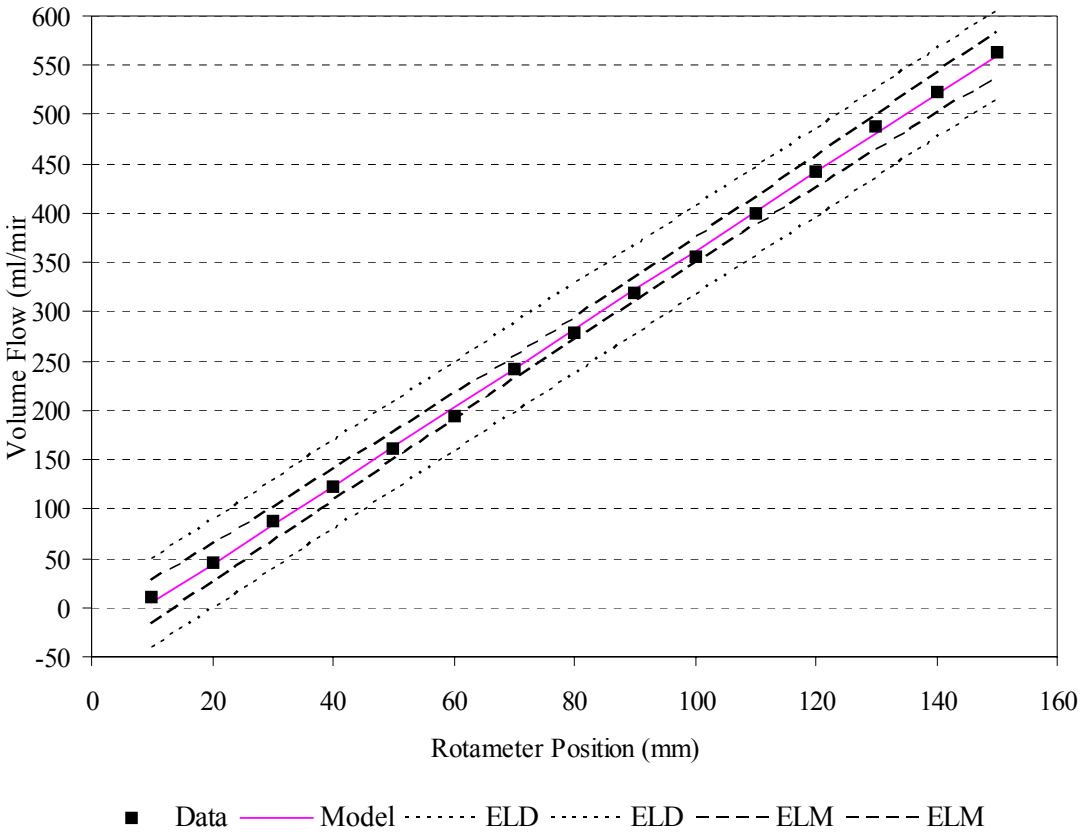

SUMMARY OUTPUT (Position vs Volumetric Flow Rate)

Regression Statistics	
Multiple R	0.999702
R Square	0.999403
Adjusted F	0.999357
Standard E	4.504966
Observatio	15

ANOVA

	df	*SS*	*MS*	*F*	*Significance F*
Regressior	1	441868.3902	441868.3902	21772.58125	2.3948E-22
Residual	13	263.8313302	20.29471771		
Total	14	442132.2216			

	Coefficients	*Standard Error*	*t Stat*	*P-value*	*Lower 95%*	*Upper 95%*	*Lower 95.0%*	*Upper 95.0%*
Intercept	-35.40859	2.447810001	-14.46541546	2.1583E-09	-40.69675961	-30.12041764	-40.69675961	-30.12041764
X Variable	3.972532	0.026922321	147.5553498	2.3948E-22	3.914370307	4.03069456	3.914370307	4.03069456

A.3 Differential Pressure Transducer Calibration Data

Differential Pressure Transducer Calibration Data			
Current	Pressure Measured	Pressure Calculated	Model
mA	in H2O	in H2O	in H2O
3.982	0.00	0.00	0.01
4.159	0.07	1.20	1.24
4.480	2.02	3.47	3.46
4.763	3.24	5.57	5.42
4.997	4.07	7.00	7.03
5.210	4.95	8.51	8.51
5.444	5.87	10.10	10.13
5.744	7.10	12.21	12.20
5.968	8.05	13.85	13.75
6.243	9.10	15.65	15.65
6.455	9.95	17.11	17.12
6.709	10.97	18.87	18.87
6.973	12.04	20.71	20.70
7.270	13.24	22.77	22.75
7.509	14.16	24.36	24.41
7.730	15.10	25.97	25.94
7.894	15.75	27.09	27.07
8.174	16.88	29.03	29.01
8.523	18.27	31.42	31.42
8.734	19.10	32.85	32.88
8.885	19.72	33.92	33.92
9.251	21.10	36.29	36.46
9.388	21.72	37.36	37.40
9.704	23.02	39.59	39.59
10.010	24.27	41.74	41.70
10.365	25.68	44.17	44.16
10.699	27.00	46.44	46.47
11.020	28.24	48.57	48.69
11.194	29.02	49.91	49.89
11.466	30.10	51.77	51.77
11.690	31.00	53.32	53.32
11.962	32.08	55.18	55.20
12.237	33.20	57.10	57.11
12.369	33.72	58.00	58.02
12.672	34.95	60.11	60.12
12.933	36.00	61.92	61.92
13.120	36.76	63.23	63.21
13.354	37.70	64.84	64.83
13.619	38.74	66.63	66.66
13.919	39.99	68.78	68.74
14.108	40.76	70.11	70.05
14.415	41.98	72.21	72.17
14.586	42.67	73.39	73.35
14.897	43.90	75.51	75.50
15.080	44.62	76.75	76.77
15.360	45.77	78.72	78.71
15.670	47.00	80.84	80.85
15.815	47.59	81.85	81.85
16.132	48.86	84.04	84.04
16.361	49.80	85.66	85.63

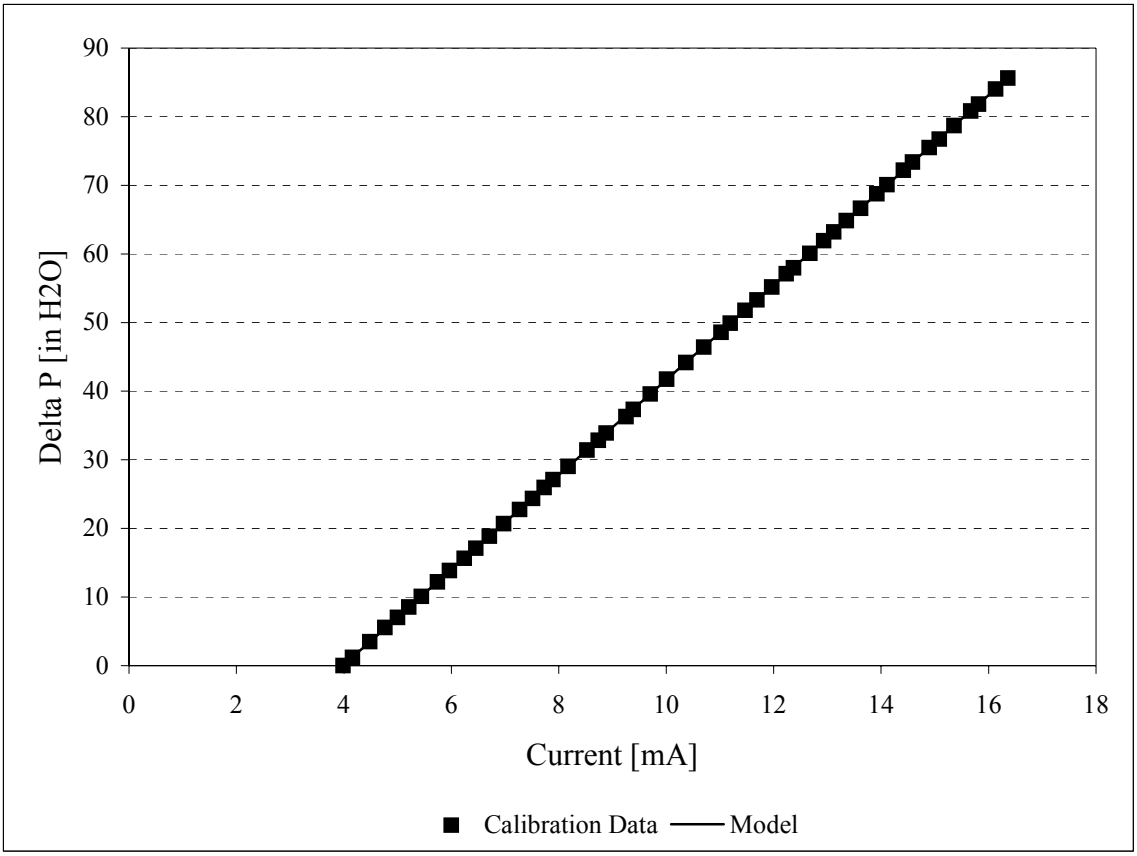

SUMMARY OUTPUT

Regression Statistics	
Multiple R	0.999998411
R Square	0.999996823
Adjusted R Square	0.999996757
Standard Error	0.046283933
Observations	50

ANOVA

	df	*SS*	*MS*	*F*	*Significance F*
Regression	1	32363.60095	32363.60095	15107629.44	1.2826E-133
Residual	48	0.102825718	0.002142202		
Total	49	32363.70378			

	Coefficients	*Standard Error*	*t Stat*	*P-value*	*Lower 95%*	*Upper 95%*	*ower 95.0%*	*Upper 95.0%*
Intercept	-27.52482594	0.019268132	-1428.515566	9.4217E-113	-27.5635671	-27.48608	-27.56357	-27.48608
X Variable 1	6.916032188	0.00177934	3886.853412	1.2826E-133	6.912454588	6.91961	6.912455	6.91961

A.4 Precision Uncertainty in Digital Measurements

	T1	T2	T3	T4	T5	T6	WBD6
	C	C	C	C	C	C	C
	20.775	70.044	78.192	52.752	52.049	60.449	7.094
	20.751	70.057	78.185	52.759	52.141	60.429	7.101
	20.757	70.059	78.192	52.772	52.055	60.450	7.126
	20.745	70.017	78.199	52.773	52.186	60.449	7.126
	20.749	70.059	78.184	52.803	52.069	60.428	7.167
	20.707	70.043	78.205	52.769	52.126	60.441	7.159
	20.719	70.047	78.181	52.796	52.082	60.438	7.140
	20.735	70.029	78.198	52.782	52.085	60.399	7.142
	20.752	70.023	78.166	52.767	52.100	60.422	7.133
	20.730	70.026	78.179	52.733	52.031	60.421	7.169
sum	207.420	700.404	781.881	527.706	520.924	604.326	71.357
average	20.742	70.040	78.188	52.771	52.092	60.433	7.136
SSD	0.020	0.016	0.011	0.020	0.047	0.016	0.025
k	2.262	2.262	2.262	2.262	2.262	2.262	2.262
U	0.014	0.011	0.008	0.015	0.034	0.012	0.018

	T7	T8	T9	Tboiler	Toil	dP7	RH1
	C	C	C	C	C	in H2O	fraction
	153.295	20.154	70.497	22.455	67.470	8.762	0.061
	153.271	20.194	70.517	22.448	67.429	8.801	0.061
	153.252	20.254	70.552	22.436	67.438	8.815	0.065
	153.218	20.121	7.519	22.432	67.432	8.878	0.060
	153.158	20.154	70.514	22.419	67.438	8.796	0.060
	153.261	20.152	70.509	22.415	67.429	8.831	0.060
	153.277	20.187	70.517	22.440	67.399	8.851	0.060
	153.246	20.213	70.565	22.417	67.447	8.844	0.060
	153.234	20.167	70.569	22.436	67.405	8.791	0.060
	153.231	20.241	70.637	22.418	67.423	8.821	0.061
sum	1532.443	201.837	642.396	224.316	674.310	88.190	0.608
average	153.244	20.184	64.240	22.432	67.431	8.819	0.061
SSD	0.038	0.042	19.930	0.014	0.020	0.034	0.002
k	2.262	2.262	2.262	2.262	2.262	2.262	2.262
U	0.027	0.030	14.257	0.010	0.014	0.024	0.001

n = 10

The above columns of data are successive measurements that were taken at steady state operation. Uncertainty due to precision error, or U_A, was determined from this data using Equation 4.2.

Appendix B

Vane Angle Calculations

B.1 Vane Height Calculations

Inputs				
In Pipe Dia (in.)	Model Dia (in.)	Mill Bit Size (in.)	Lip Size (in.) (desired)	Cut Depth (in)
2.000	3.000	0.500	0.063	0.000
2.000	3.000	0.500	0.063	0.000
2.000	3.000	0.500	0.063	0.100
2.000	3.000	0.500	0.063	0.250
2.000	3.000	0.500	0.063	0.150
2.000	3.000	0.500	0.063	0.200
2.000	3.000	0.500	0.063	0.175

Vanes intersect. Therefore, try 15 vanes and a deeper cut to preserve flow area.

2.000	3.000	0.500	0.063	0.250
2.000	3.000	0.500	0.063	0.200

Calculations						
Cent Ang (deg)	T. Height (in.)	Sec Area (in.^2)	T. Area (in.^2)	Sliver	In Pipe A (in.^2)	Vane Area
19.188	1.479	0.377	0.370	0.007	3.142	1.762
19.188	1.479	0.377	0.370	0.007	3.142	1.683
19.188	1.479	0.377	0.370	0.007	3.142	2.483
19.188	1.479	0.377	0.370	0.007	3.142	3.683
19.188	1.479	0.377	0.370	0.007	3.142	2.883
19.188	1.479	0.377	0.370	0.007	3.142	3.283
19.188	1.479	0.377	0.370	0.007	3.142	3.083

19.188	1.479	0.377	0.370	0.007	3.142	3.453
19.188	1.479	0.377	0.370	0.007	3.142	3.078

Results			
Model Perim (in.	# Vanes	Lip Size (in.) (Act	(Pipe - Vane)
9.425	16.755	0.062	1.379
9.425	16.000	0.084	1.459
9.425	16.000	0.084	0.659
9.425	16.000	0.084	-0.541
9.425	16.000	0.084	0.259
9.425	16.000	0.084	-0.141
9.425	16.000	0.084	0.059

9.425	15.000	0.113	-0.311
9.425	15.000	0.113	0.064

B.2 Vane Angle Calculation

$$\omega = 2u$$

$$\tan \alpha = \frac{\omega}{u}$$

$$\alpha = \tan^{-1}\left(\frac{35}{17.5}\right) = 63.4\ ^\circ$$

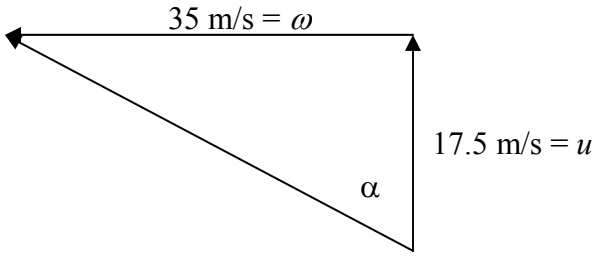

Appendix C

EES Program Listing

```
"Station 1: Air Supply"
"Station 2: Heated dry air"
"Station 3: Mixed air and steam (Turbine Inlet)"
"Station 4: Turbine Outlet"
"Station 5: Exhaust to atmosphere (after separator)"
"Station 6: Throttled mixture to RH probe"
"Station 7: Steam inlet (before F.O.)"
"Station 8: Compressor Inlet"
"Station 9: Compressor Outlet"

"Inputs"

"T[1]=20.7                          [C]"
"T[2]=20.8                          [C]"
"T[3]=77.0                          [C]"
"T[4]=51.2                          [C]"
"T[5]=51.2                          [C]"
"T[6]=49.3                          [C]"
"WBD_6                              [C] wet bulb depression"
"T[7]=149.3                         [C]"
"T[8]=20.2                          [C]"
"T[9]=97.5                          [C]"
"T_boiler_in                        [C]"

"P[1]=53.5                          [psig]"
"RM[1]=75                           indicated position"
"P[3]=26.5                          [psig]"
"dP[4]=11.1                         [inH2O]"
"P[7]=53.0                          [psig]"
"P[9]=11.4                          [psig]"
"RM[9]=60.3                         indicated position"
"P_boiler=68                        [psig]"
"dP[7]=38.5                         [inH2O]"
"P_atm=741                          [mmHg]"
"Q_measured=0.715                   [kW] this is actually 1/4 of the total power"
"phi_1_throttled=0.007              fractional value of relative humidity measured of
throttled, unheated air"
"phi_8=0.56                         fractional relative humidity of ambient air"


procedure phaseselector(RH_in:RH_out,liqmult)
        if(RH_in<1.0) then
                RH_out=RH_in
                liqmult=0
        else
                RH_out=1.0
```

```
            liqmult=1
        ENDif
end

procedure focalc(H_orIFice,T_amb,T_fluid,P_fluid_psig,P_fluid_kPa,P_amb_psia:m_dot_fluid,C)
        if(H_orifice=0) then
            m_dot_fluid=0
            C=0
        else
            "Geometric characteristics of flow orifice"
            D=0.822
            "[in] pipe inside diameter"
            d_t=0.315
            "[in] orfice diameter"
            Beta=d_t/D
            "ratio of orifice diameter to inside pipe diameter"
            A_D=(pi*D^2/4)*convert(in2,m2)
            "[m2] x-sectional area of pipe"
            A_d_t=(pi*d_t^2/4)*convert(in2,m2)
            "[m2] area of orifice opening"

            "Thermophysical properties of steam at station 7"
            density_fluid=density(STEAM,T=T_fluid,P=P_fluid_kpa)
            kvisc_fluid=viscosity(STEAM,T=T_fluid,P=P_fluid_kpa)/density_fluid
            "[m2/s]"

            "Thermal Expansion Factor"
            alpha_P=7.2*10^(-6)
            "[in/in/F] thermal expansion coefficient of SS pipe"
            alpha_PE=11*10^(-6)
            "[in/in/F] thermal expansion coefficient of brass orifice"
            T_fluid_F=T_fluid*1.8+32
            "[F]"
            F_a=1+(2/(1-Beta^4))*(alpha_PE-Beta^4*alpha_P)*(T_fluid_F-T_amb)
            "Thermal expansion factor"

            "Fluid Compressibility Factor"
            k=cp(STEAM,T=T_fluid,P=P_fluid_kPa)/cv(STEAM,T=T_fluid,P=P_fluid_kPa)
        "specific heat ratio of the fluid"
            Y_1=1-(0.41+0.35*Beta^4)*(H_orifice/(27.73*k*(P_fluid_psig+P_amb_psia)))
        "Expansion factor based on upstream pressure"

            "Discharge Coefficient"
            i=0
            j=1
            dP_fluid=H_orifice*convert(inH2O,Pa)          "[Pa]"

            repeat
                i=i+1
                if(i=1) then
                    Velocity_fluid[j]=5                                          "[m/s]"
                else
                    Velocity_fluid[j+1]=(Velocity_fluid[j-1]+9*Velocity_fluid[j])/10
                endif
```

```
                    Re_D_fluid=(Velocity_fluid[j]*D*convert(in,m)/kvisc_fluid)"Reynold's
number of fluid"
                    lambda=1000/(Re_D_fluid)^0.5

        K_SB=(0.5991+0.0044/D+(0.3155+0.0175/D)*(Beta^4+2*Beta^16))+(0.00052/D-
0.000192+(0.01648-0.00116/D)*(Beta^4+4*Beta^16))*lambda
                    C=K_SB*(1-Beta^4)^0.5
                "Impirical Discharge Coefficient"
                    V_dot_fluid[j]=C*Y_1*F_a*A_d_t*((2*dP_fluid)/(density_fluid*(1-
Beta^4)))^0.5                    "[m3/s]"
                    j=j+1
                    Velocity_fluid[j]=V_dot_fluid[j-1]/A_D                    "[m/s]"
                    error=(Velocity_fluid[j]-Velocity_fluid[j-1])/Velocity_fluid[j] "convergence
criteria"
                until(abs(error)<0.001)
                m_dot_fluid=V_dot_fluid[j-1]*density_fluid                    "[kg/s]"

        ENDif
end

Procedure boilerpowerflow(H_orIFice,T_in,T_out,P_in,P_out:m_dot_power)
        if(H_orifice=0) then
                m_dot_power=0
                "[kg/s]"
        else
                Q=207*48*3^0.5*10^(-3)          "[kW] 3 phase electric power delivered to boiler
for 207V line to line and 48 A per leg"
                h_in_boiler=enthalpy(STEAM,T=T_in,P=P_in)          "enthalpy of water into
boiler"
                h_out_boiler=enthalpy(STEAM,T=T_out,P=P_out)          "enthalpy of
steam out of boiler"
                m_dot_power=Q/(h_out_boiler-h_in_boiler)          "energy equation for
boiler, gives mass flow rate"
        ENDif
end

procedure
revturbentropy(w_out_2p,s_mix_out_2p,m_dot_liq_2p,S_dot_in,w_in,P_out,m_dot_air:S_dot_ou
t,m_dot_liq_out,s_mix_out,w_out_s)
        if(m_dot_liq_2p<0.0) then
                m_dot_liq_out=0.0

                w_out_s=w_in
                S_dot_out=S_dot_in
                s_mix_out=S_dot_out/m_dot_air
        else
                m_dot_liq_out=m_dot_liq_2p
                w_out_s=w_out_2p
                S_dot_out=S_dot_in
                s_mix_out=s_mix_out_2p
        ENDif
end

procedure
revturbwork(P_out,T_out_s,w_out_s,W_dot_turb_s_2p,H_out_s_2p,m_dot_liq_2p,eta_turbine_2
p,H_in,m_dot_air,W_dot_turb:W_dot_turb_s,H_out_s,eta_turbine_s)
```

```
        if(m_dot_liq_2p<0.0) then
                h_out_mix_s=enthalpy(AIRH2O,T=T_out_s,P=P_out,w=w_out_s)
                H_out_s=m_dot_air*h_out_mix_s
                                        "[kW]"
                W_dot_turb_s=H_in-H_out_s
                eta_turbine_s=W_dot_turb/W_dot_turb_s
        else
                W_dot_turb_s=W_dot_turb_s_2p
                H_out_s=H_out_s_2p
                eta_turbine_s=eta_turbine_2p
        ENDif
end

"Pressure conversions"
P_atm_kpa=P_atm*convert(mmHg,kpa)                       "[kpa]"
P_atm_psi=P_atm*convert(mmHg,psi)                       "[psi]"
P_kpa[1]=P[1]*convert(psi,kpa)+P_atm_kpa                "[kpa]"
P_kpa[3]=P[3]*convert(psi,kpa)+P_atm_kpa                "[kpa]"
P_kpa[4]=dP[4]*convert(inH2O,kpa)+P_atm_kpa             "[kpa]"
P_kpa[7]=P[7]*convert(psi,kpa)                          "[kpa]"
P_kpa[9]=P[9]*convert(psi,kpa)+P_atm_kpa                "[kpa]"
P_boiler_kpa=P_boiler*convert(psi,kpa)+P_atm_kpa        "[kpa]"

"Air Mass Flow (1 and 9)"
Density_std=density(AIR,T=20,P=101)
T_1_std=294.44                                                          "[K]"
P_1_std=46.7                                                            "[psia]"
P_1_abs=P[1]+P_atm_psi                                                  "[psia]"
F_SCFM[1]=RM[1]*((P_1_abs*T_1_std)/(P_1_std*(T[1]+273.15)))^0.5         "mass flow"
Density_1=density(AIR,T=T[1],P=P_kpa[1])
F_cfm_1=(Density_std/Density_1)*F_SCFM[1]                               "[cfm] Vol Flow"
F_m3s_1=F_cfm_1*convert(cfm,m^3/s)                                      "[m3/s] Vol
flow"
m_dot[1]=F_m3s_1*Density_1                                              "[kg/s]"

m_dot_thermal[1]=Q_measured*4/(T[2]-T[1])


T_9_std=298.00          "[K]"
P_9_std=14.7            "[psia]"
P_9_abs=P[9]+P_atm_psi                                  "[psia]"
F_9_meas_scfm=0.7275*RM[9]+2.3896
F_SCFM[9]=F_9_meas_scfm*((P_9_abs*T_9_std)/(P_9_std*(T[9]+273.15)))^0.5 "mass flow"
Density_9=density(AIR,T=T[9],P=P_kpa[9])
F_cfm_9=(Density_std/Density_9)*F_SCFM[9]               "[cfm] vol flow"
F_m3s_9=F_cfm_9*convert(cfm,m^3/s)                              "[m3/s] vol flow"
m_dot[9]=F_m3s_9*Density_9      "[kg/s]"



"Steam Mass Flow"
"Calls function 'focalc' to calculate the steam flow rate.  Returns steam mass flow of 0 if dp[7] is
0"
call focalc(dP[7],T_atm,T[7],P[7],P_kPa[7],P_atm_psi:m_dot[7],C)
```

```
"Theoretical Steam Mass Flow and Temperature"
Call boilerpowerflow(dP[7],T_boiler_in,T[7],P_boiler_kPa,P_kPa[7]:m_dot_theoretical[7])

"Liquid Water Flowrate to Boiler"
V_dot_boiler_in=(4.1141*RM_boiler-49.267)*convert(mL/min,m^3/s)      "[m3/s] Volumetric flow
of water from calibrated rotameter"
density_boiler_in=density(STEAM,T=T_boiler_in,P=P_boiler_kPa)        "Density of water
entering boiler"
m_dot_boiler_in=V_dot_boiler_in*density_boiler_in                    "Mass flow of water into
boiler"

"Wet Bulb Thermometer"
T_db=T[6]                                                            "dry bulb temp"
T_wb=T[6]-WBD_6                                                  "wet bulb temp from measured
wet bulb depression"
w_6=humrat(AIRH2O,T=T_db,P=P_atm_kPa,B=T_wb)                         "humidity ratio at 6"
w_3_wb=w_6                                                           "statement of mass
conservation, between 3 and 6"
m_dot_wb_7=(w_3_wb-w_1)*m_dot[1]              "steam mass flow rate calculated using
difference in humidiy ratios between 1 and 3"



"Theoretical T[3] Calculation"
"Vapor and Dry Air Flowrates for Station 1 and 3"
{phi_1_throttled=.11}

w_1=humrat(AIRH2O,T=T[1],P=P_atm_kpa,R=phi_1_throttled)  "humidity ratio of throttled air at
1"
phi_1=relhum(AIRH2O,T=T[1],P=P_kPa[1], W=w_1)                "relative humidity of pressurized
air at 1"
m_dot_vap_1=m_dot[1]/(1/w_1+1)                                                "mass
flow rate of water vapor in air at 1"
m_dot_da=m_dot[1]/(w_1+1)                                                     "mass
flow rate of dry air at 1"
m_dot_vap_3=m_dot_steam+m_dot_vap_1                                  "mass flow rate of
water vapor at station 3 due to added steam"
w_3_orifice=m_dot_vap_3/m_dot_da                                              "humidity ration
at 3 using orifice gauge steam mass flow rate"

"Mass and Energy Losses"
"These equations account for the loss of heat in the heated air line and the loss of condensate in
the boiler steam trap"
{m_dot_ST=1.6/60000}
                    "[kg/s] Measured drip out of steam trap"
m_dot_steam=m_dot[7]-m_dot_ST/60000                                           "[kg/s]
Mass flow of steam after steam trap"
Q_dot_23=UA_23*LMTD
                    "[kW] Heat lost to ambient"
LMTD=((T[3]-T_atm)-(T[2]-T_atm))/ln((T[3]-T_atm)/(T[2]-T_atm))       "[C] LMTD for HE with
ambient air"
UA_23=0.001328
                                  "[kW/C] experimental UA from 2 to 3"

"Energy Balance for Mixing"
```

```
h_mixture=(m_dot_da*h_2+(m_dot_steam)*h_7-Q_dot_23)/m_dot_da    "[kJ/kg_da] Calculated
enthalpy of mix"
h_2=enthalpy(AIRH2O,T=T[2],P=P_kpa[1],w=w_1)                    "[kJ/kg_da] enthalpy of
heated air at 2"
h_7=enthalpy(STEAM,T=T[7],P=P_kPa[7])                                    "[kJ/kg]
enthalpy of steam at 7, note constant enthalpy boiling into system"
T_theory_3=temperature(AIRH2O,h=h_mixture,P=P_kpa[3],w=w_3_orifice)      "[C] theoretical
temp at 3"
phi_3=relhum(AIRH2O,T=T[3],P=P_kpa[3],w=w_3_orifice)                    "Calculated
fractional RH at 3"



"Compressor Work"
h[8]=enthalpy(AIR,T=T[8])
        "enthalpy of air (ideal) at 8"
h[9]=enthalpy(AIR,T=T[9])
        "enthalpy of air (ideal) at 9"
W_dot_compressor=m_dot[9]*(h[9]-h[8])                                    "[kW]
compressor work"
s[8]=entropy(AIR,T=T[8],P=P_atm_kpa)                                    "entropy at 8"
T_s[9]=temperature(AIR,s=s[8],P=P_kpa[9])                               "isentropic temperature
at 9"
h_s[9]=enthalpy(AIR,T=T_s[9])
        "isentropic enthalpy at 9"
W_dot_compressor_s=m_dot[9]*(h_s[9]-h[8])                               "[kW] isentropic
compressor work"
Eta_compressor_s=W_dot_compressor_s/W_dot_compressor   "isentropic compressor
efficiency"

"Turbine Work"
w_3=w_3_orifice          "the humidity ratio at 3 is defined, can be switched to humity ratio
defined by wet bulb measurement"
RH_4=relhum(AIRH2O,P=P_kPa[4],T=T[4],W=w_3)      "fractional relative humidity at 4"
call phaseselector(RH_4:phi[4],liqmult)              "function 'phaseselector' determines the phase
at state 4 for the turbine work calculation"

        "'phaseselector' returns the relative humidity at 4 and multiplier for the liquid mass at 4"
"energy"
W_dot_turbine=H_3-H_4
                "[kW] turbine energy balance"
H_4=m_dot_da*h_4_mix+m_dot_liq_4*h_4_liq                                "[kW] extensive
enthalpy at 4"
H_3=m_dot_da*h_3_mix
                "[kW] extensive enthalpy at 3"
h_4_mix=enthalpy(AIRH2O,T=T[4],P=P_kpa[4],w=w_4_mix)     "enthalpy of mixture at 4"
h_4_liq=enthalpy(STEAM,T=T[4],P=P_kpa[4])                       "enthalpy of liquid at 4"

h_3_mix=enthalpy(AIRH2O,T=T[3],P=P_kpa[3],w=w_3)          "[kJ/kg_da] enthalpy of mixture
at 3"

"entropy"
S_dot_3=m_dot_da*s_3
                "[kW/C] extensive entropy at 3"
s_3=entropy(AIRH2O,T=T[3],P=P_kPa[3],w=w_3)                             "intensive entropy at 3"
```

```
"mass"
w_4_mix=humrat(AIRH2O,T=T[4],P=P_kpa[4],R=phi[4])          "humidity ratio at 4"
m_dot_liq_4=m_dot_da*(w_3-w_4_mix)*liqmult                 "[kg/s] mass balance
determines mass flow rate of liquid at 4"
m_dot_water=m_dot_liq_4*convert(kg/s,g/min)                "[g/min]"

"Reversible Turbine"
"First assume 2 phase at station 4 (RH=100%) and calculate the isentropic turbine work with the
following equations"
"The phase is checked in function 'revturbentropy' after EES solves the 2 phase case"
"EES finds T_4_s by using the following 'entropy' and 'mass' groups of equations"
"entropy"
S_dot_4=S_dot_3
                    "[kW/K] extensive entropy at 4 is equal to 3 in isentropic case"
S_dot_4=m_dot_da*s_mix_4_s+m_dot_liq_4_s*s_liq_4_s         "[kW/K] statement of extensive
entropy at 4"
s_liq_4_s=entropy(STEAM,T=T_4_s,x=0)                                    "[kJ/(kg*K)]
entropy of liquid at 4"
s_mix_4_s=entropy(AIRH2O,T=T_4_s,P=P_kPa[4],w=w_4_s)   "[kJ/(kg*K)] entropy of the
air/vapor mixture at 4(isentropic)"

"mass"
w_4_s=humrat(AIRH2O,T=T_4_s,P=P_kPa[4],R=1)                "[kgw/kga] humidity ratio at
4(isentropic)"
m_dot_liq_4_s=m_dot_da*(w_3-w_4_s)                              "[kg/s] mass flowrate of
liquid water at 4(isentropic)"

"energy"
W_dot_turbine_s=H_3-H_4_s                                                    "[kW]"
H_4_s=m_dot_da*h_4_mix_s+m_dot_liq_4_s*h_4_liq_s           "[kW] extensive enthalpy at 4
(isentropic)"
h_4_mix_s=enthalpy(AIRH2O,T=T_4_s,P=P_kpa[4],w=w_4_s)  "[kJ/kg]  enthalpy of the
air/vapor mixture at 4(isentropic)"
h_4_liq_s=enthalpy(STEAM,T=T_4_s,x=0)                                   "[kJ/kg]
enthalpy of the liquid at 4(isentropic)"
eta_turbine_s=W_dot_turbine/W_dot_turbine_s                "dimensionless isentropic
turbine efficiency"

"Now test the phase, if single phase calculate s_mix_4_rev with function 'revturbentropy' then
implicitly calculate T_4_rev with result"
call
revturbentropy(w_4_s,s_mix_4_s,m_dot_liq_4_s,S_dot_3,w_3,P_kPa[4],m_dot_da:S_dot_4_rev
,m_dot_liq_4_rev,s_mix_4_rev,w_4_rev)
s_mix_4_rev=entropy(AIRH2O,T=T_4_rev,P=P_kPa[4],w=w_3)

"The function revturbwork outputs the reversible turbine work for either a 1 or 2 phase state at
station 4"
call
revturbwork(P_kPa[4],T_4_rev,w_4_rev,W_dot_turbine_s,H_4_s,m_dot_liq_4_s,eta_turbine_s,H
_3,m_dot_da,W_dot_turbine:W_dot_turbine_rev,H_4_rev,eta_turbine_rev)

"Bearing Work"
UA_oil=10.41
                          "[W/C] UA of oil reservoir is found experimentally"
W_dot_bearing=(UA_oil*(T_oil-T_atm)-W_dot_pump)/1000       "[kW] work bearing dissipates in
oil reservoir"
```

```
"Dummy Variables"
phi_atm=phi_8                                   "phi_atm not used in program, but is in table"
T_3_compare=T[3]                                "dummy variable for table"
P_3_compare=P[3]                                "dummy variable for table"

"Separation Efficiency"
"m_dot_sep=15"
eta_sep=m_dot_sep/m_dot_water

"wet-bulb accuracy"
dif_OFM_WB=100*(abs(m_dot_steam-m_dot_wb_7))/m_dot_steam
```

Appendix D

Experimental Data

Experimental Data: Trials 1-10 Max Settling Length, Trials 11-20 Min Settling Length, Trials 21-25 Mid Settling Length

Trial	RM_1	ϕ_1	T_1	T_2	T_4	T_7	T_{atm}
	scfm	%	ºC	ºC	ºC	ºC	ºC
1	80	0.148	20.45	66.00	55.00	160.6	23.5
2	80	0.140	20.53	62.00	54.35	160.9	23.5
3	80	0.141	20.50	57.50	54.41	160.3	23.5
4	80	0.142	20.60	53.00	54.23	160.3	23.5
5	80	0.143	20.50	49.70	54.21	160.2	23.5
6	80	0.143	20.60	40.00	53.83	160.1	23.5
7	80	0.142	20.60	35.50	53.20	160.1	23.5
8	80	0.143	20.60	29.80	53.03	160.0	23.5
9	79	0.143	20.50	26.50	52.71	159.8	23.5
10	78	0.143	20.50	21.00	52.40	159.7	23.5
11	79	0.148	21.30	71.20	57.25	160.6	20.0
12	79	0.140	21.20	66.62	56.70	160.9	20.0
13	79	0.141	21.10	62.20	56.40	160.3	20.0
14	78	0.142	20.90	57.65	56.30	160.3	20.0
15	80	0.143	21.10	52.76	55.70	160.2	20.0
16	80	0.143	20.90	49.48	55.30	160.1	20.0
17	80	0.142	20.80	43.06	54.95	160.1	20.0
18	80	0.143	20.84	40.37	54.65	160.0	20.0
19	80	0.143	20.80	35.48	54.35	159.8	20.0
20	80	0.143	20.80	30.19	54.15	159.7	20.0
21	80	0.148	20.45	66.00	55.00	160.6	19.8
22	80	0.140	20.53	57.50	54.30	160.9	19.8
23	80	0.141	20.50	42.00	54.62	160.3	19.8
24	80	0.142	20.60	30.10	54.22	160.3	19.8
25	80	0.143	20.50	20.52	52.20	160.2	19.8
Conventional	80	0.147	20.70	66.00	55.00	158.9	20.5
Separator	80	0.147	20.70	25.00	52.20	158.9	20.3

Experimental Data

Trial	P_{atm}	P_1	P_4	P_7	ΔP_7	ΔP_5	$\dot{m}_{sep}$	$\dot{m}_{liq}$
	mmHg	psi	in.H_2O	psi	in. H_2O	in.H_20	g/min	g/min
1	737.6	41.0	31.04	75.00	24.6	7.0	18.03	20.41
2	737.6	41.0	31.04	73.00	24.3	6.7	22.03	24.67
3	737.6	40.0	31.04	74.50	24.7	6.7	28.40	32.97
4	737.6	40.0	30.78	74.50	24.9	6.7	34.44	37.35
5	737.6	39.8	30.78	75.80	25.5	6.7	39.65	45.41
6	737.6	39.1	30.78	75.50	25.3	6.7	48.00	51.79
7	737.6	39.0	30.78	75.00	25.3	6.6	54.31	61.07
8	737.6	38.9	30.78	75.00	25.2	6.6	58.52	63.46
9	737.6	38.0	30.72	75.00	25.1	6.6	66.00	73.42
10	737.6	38.0	30.72	75.10	25.0	6.6	75.00	81.00
11	739.9	40.5	31.85	81.00	27.0	7.1	15.00	16.28
12	739.9	40.5	31.04	80.50	26.2	7.1	18.00	19.05
13	739.9	40.0	30.51	79.50	26.3	7.1	22.20	24.42
14	739.9	39.8	31.58	80.00	26.3	7.1	28.20	33.29
15	739.9	40.4	31.58	80.00	26.2	7.1	33.50	35.96
16	739.9	40.0	31.58	79.50	26.3	7.1	38.10	41.78
17	739.9	40.0	31.04	79.50	26.2	7.0	43.50	46.75
18	739.9	40.0	30.51	79.40	26.2	7.0	47.60	51.49
19	739.9	40.0	30.51	79.25	26.1	6.9	51.73	55.37
20	739.9	39.5	29.97	78.78	26.1	7.0	56.20	58.97
21	737.6	41.0	31.04	75.00	24.6	7.0	18.40	20.41
22	737.6	41.0	31.04	73.00	24.3	7.0	21.90	25.54
23	737.6	40.0	31.04	74.50	24.7	7.0	27.19	29.31
24	737.6	40.0	30.78	74.50	24.9	6.9	35.18	37.52
25	737.6	39.8	30.78	75.80	25.5	6.9	67.90	77.85
Conventional	737.6	40.5	29.97	76.75	26.0	21.3	11.97	18.42
Separator	737.6	40.5	29.97	76.75	26.0	20.8	20.80	32.50

References

Abbott, Ira H.; von Doenhoff, Albert E.; and Stivers, Louis S., "Summary of Airfoil Data", NACA Report 824, 1945.

Amphlett, et al., "The Operation of a Solid Polymer Fuel Cell: A Parametric Model," Royal Military College of Canada, 1993.

ASHRAE Standard, "Standard Methods for Measurement of Moist Air Properties," pp.19-21, American Society of Heating, Refrigeration, and Air Conditioning Engineers, 1982.

Avci, A.; Karagoz, I., "A Mathematical Model for the Determination of a Cyclone Performance," Int. Comm. Heat Mass Transfer, Vol. 27, No. 2, 0735-1933 pp.263-272, 2000.

Bean, H.S., ed., "Fluid Meters: Their Theory and Application, 6th Ed., American Society of Mechanical Engineers, New York, 1971.

EG&G Technical Services, Inc.; Science Applications International Corporation, "Fuel Cell Handbook", Sixth Edition, U.S. Department of Energy, National Energy Technology Laboratory, 2002.

Hirschenhofer, J.H.; D.B. Stauffer; R.R. Engelman; and M.G. Klett., "Fuel Cell Handbook", Fourth Edition. Parsons Corp. 1998

Jeter, S. M., "Microsoft Visual Basic User Form for Plotting Error Limits of Regression Models", The George W. Woodruff School of Mechanical Engineering, Georgia Institute of Technology, Atlanta GA 30332-0405, 2004.

Ladson, Charles L.; Brooks, Cuyler W.; Jr., Hill, Acquilla S.; and Sproles, Darrell W., "Computer Program To Obtain Ordinates for NACA Airfoils", NASA Technical Memorandum 4741, 1996.

Mctaggert, “Advanced Fuel Cells for Automotive Applications – Development of a Compressor/Expander for Fuel Cells in Automotive Applications,” Department of Energy, Arthur D. Little, Inc., 1998.

Nieuwstadt, F. T. M.; Dirkzwager, M., “A Fluid Mechanics Model for an Axial Cyclone Separator,” Ind. Eng. Chem. Res.; Vol. 34, No. 10, 3399-3404, 1995